

UNCLASSIFIED

AD 273 724

*Reproduced
by the*

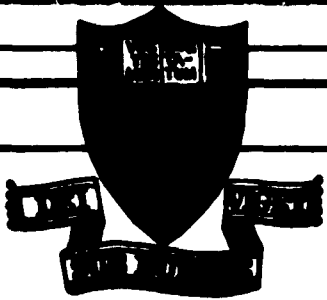
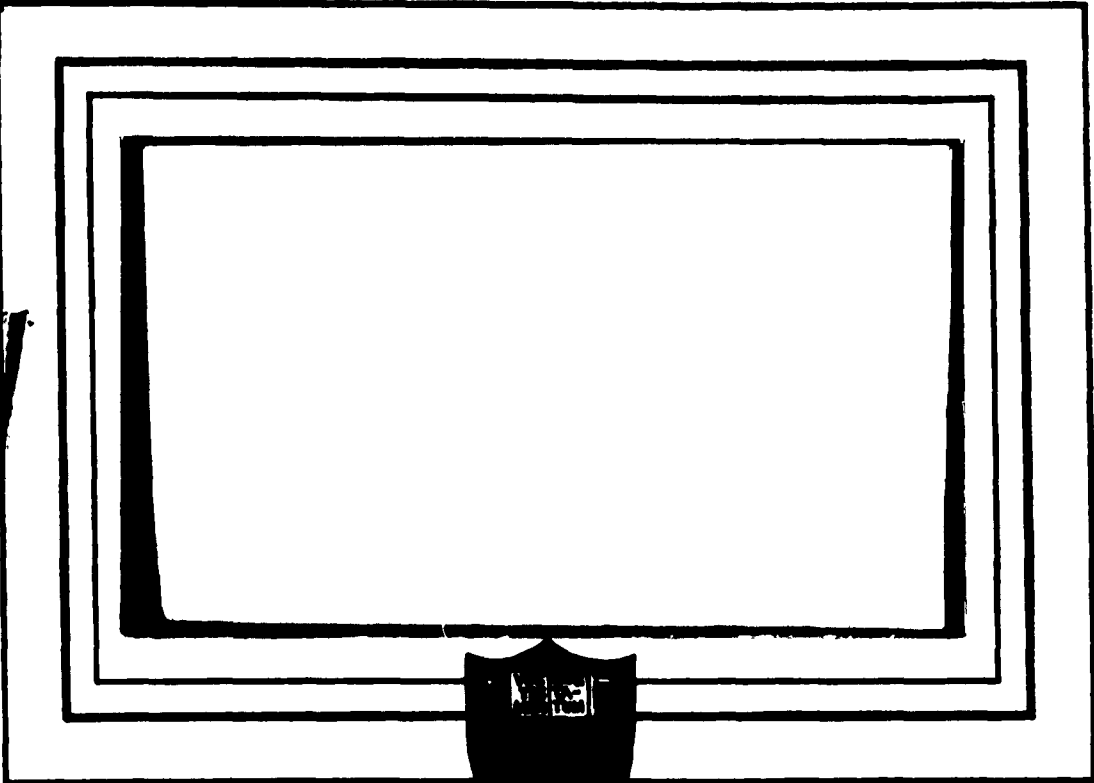
**ARMED SERVICES TECHNICAL INFORMATION AGENCY
ARLINGTON HALL STATION
ARLINGTON 12, VIRGINIA**



UNCLASSIFIED

NOTICE: When government or other drawings, specifications or other data are used for any purpose other than in connection with a definitely related government procurement operation, the U. S. Government thereby incurs no responsibility, nor any obligation whatsoever; and the fact that the Government may have formulated, furnished, or in any way supplied the said drawings, specifications, or other data is not to be regarded by implication or otherwise as in any manner licensing the holder or any other person or corporation, or conveying any rights or permission to manufacture, use or sell any patented invention that may in any way be related thereto.

273 724
AS AD NO. 273724
ASTIA



APR 4 1962
62-2-6
ASTIA

PRINCETON UNIVERSITY
PLASTICS LABORATORY

PLASTICS LABORATORY

TECHNICAL REPORT

No. 64B

SEMICONDUCTION IN METAL-DOPED

PYRO-POLYMERS

S. L. Rosen & H. A. Pohl

15 January 1962

Contract No. DA-36-039sc-89143

ONR-NR 356-375

"Reproduction, translation, publication use and disposal in whole or in part by or for the United States Government is permitted".

The work reported here was supported partly by the Army, Navy and Air Force under Signal Corps Contract DA-36-039sc-78105; DA Project 3A00-15-001; ONR Project NR 356-375.

ABSTRACT

The electronic properties of pyrolysis products of sodium-, calcium- and thorium-doped ion-exchange resins were investigated. The resulting pyro-polymers are degenerate semiconductors whose resistivities decrease from approximately 0.1 to 0.01 ohm-cm as the pyrolysis temperature is increased from 800 to 1200°C. Resistivities can be altered roughly by a factor of two with appropriate doping.

The materials exhibit the negative resistivity-temperature behavior common to semi-conductors, and have small (.005 to .05 ev) energy gaps. Small, negative (0 to - .05 cm³/coul) Hall coefficients were observed.

Carrier concentrations are estimated at approximately $1-3 \times 10^{20}$ per cm³, with mobilities of 1-4 cm²/volt-sec.

INTRODUCTION

This study is an extension of previous work done in this laboratory with nickel and aluminum-doped pyro-polymers.^{1,2} Sodium, calcium and thorium-doped materials have been investigated to determine the effects of mono-, di-, and tetravalent metals on the electronic properties of the pyro-polymers, and if possible, to shed some light on the conduction mechanisms in this class of compounds.

Although the investigation of semi-conduction in organic materials has only fairly recently begun to receive serious attention, much work has been done on the subject in the past decade³.

It is felt that semi-conduction in polymers arises from a high degree of conjugation in the system. In general, two methods have been used to obtain these highly conjugated systems, (1) direct synthesis, and (2) pyrolysis. Both methods have received extensive treatment at this laboratory and elsewhere, but the latter is particularly advantageous for use in the investigation of doped polymer semi-conductors.

It has been shown that the material produced by pyrolyzing a carbon-based organic compound above 700°C is relatively independent of the nature of the starting material.^{4,5} As the pyrolysis temperature is raised, the conjugation of the system increases, until at approximately 2700 - 3000°C, the structure is essentially graphitic.

At temperatures up to 700°C, large quantities of volatiles are evolved as crosslinking and aromatization begin. As the pyrolysis temperature increases further, the condensation of the material continues, forming highly aromatic "stacked sheets" of short-range order. The structure has been likened to a sack of coins, with variations in the orientation

and size of the individual stacks.⁵ The orientation and size of the aromatic planes increases as the pyrolysis temperature is raised until the aromatic layer structure of graphite is achieved. The formation of polymer carbons has been treated in detail.^{1,2,3,6,7,8,9}

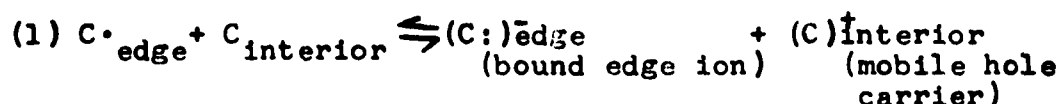
Since the pyrolysis products investigated here contain appreciable quantities of elements other than carbon (O,H,N), the term pyro-polymers would seem a more appropriate description than polymer carbons.³

The pyrolysis of doped ion-exchange resins has proved to be an experimentally effective method of introducing doping agents into the pyro-polymers. It provides a convenient method of doping with a wide variety of impurities over a controlled range of doping levels. Although no one has yet used the procedure for doping with electronegative elements, there seem to be no reasons why such a procedure would not work, using anion-exchange resins. In addition to providing an experimentally simple means of varying doping levels, this procedure does not leave a salt residue in the pyro-polymer. Such an ionic residue could contribute ionic conduction, which would interfere with investigation of the mechanisms of semi-conduction in the material. Also, the doping agents are initially atomically distributed throughout, and chemically bonded to, the carbon base material (whether they remain as such after pyrolysis is another matter).

There are, however, drawbacks to this technique, probably the most important of which is that the final pyro-polymers are heterogeneous materials. As a result, factors such as particle size, pressure, and various surface phenomena probably influence the observed electrical properties of the bulk materials. Also, the use of a binder to maintain the pyro-polymers in the form of easily handled pellets introduces some material to the aggregate which is not uniformly doped as is the rest of the material. Although these factors may

be held fairly constant while investigating a series of pyro-polymers, they introduce complications and uncertainty in trying to develop a theoretical interpretation of the electronic properties of the compounds.

The relatively high conductivity of 800°-1200°C pyro-polymers is thought to arise from the presence of a large number of charge carriers. As pyrolysis proceeds, and the material condenses into layered aromatic stacks, the removal of small molecules (CH₄, H₂O, CO₂, NH₃, etc.) leaves free radicals at the edges of the layers. These edge radicals may then produce carriers according to the following type of reaction^{2,3}



Dissociation within the layers may also produce carriers:^{2,3}



The band theory of solids has achieved outstanding success in describing inorganic semi-conductors. Applying this theory to the observed properties of pyro-polymers indicates a carrier concentration of roughly 10¹⁹⁻²⁰/cm³ (as compared with 10¹³⁻¹⁴/cm³ for germanium and 10¹¹/cm³ for silicon).^{1,3} Thus, it would be expected that much higher impurity levels would be required to affect the electronic properties of the pyro-polymers than the parts per billion needed in germanium and silicon, assuming, of course, that the impurities influence conductivity through similar mechanisms. However, the rigorous applicability of the band theory to heterogeneous, largely amorphous pyro-polymers is extremely doubtful, inasmuch as it has been developed for single crystals.

There are several ways in which doping might be expected to influence the electronic properties of pyro-polymers (considering only the metallic doping agents of valencies 1,2,3 and 4 investigated at this laboratory). As in the case of classical semi-conductors, the impurity atoms might occupy positions in the lattice of the base material (i.e., in the aromatic carbon layers of the pyro-polymers), and by capturing electrons in their deficient outer shells, create positive carriers (holes). Thorium, a tetravalent metal, would not be expected to affect conductivity through this mechanism. Alternatively, the electro-positive metals might simply contribute mobile electrons to the structure. Also, clusters of metal or compounds of the metals (oxides, carbides, nitrides, etc.) might be present, either in the aromatic planes or between them. It is conceivable that non-conducting compounds could increase the distance between aromatic planes, lowering conductivity in the direction perpendicular to the planes, and thus in the bulk material. Conductive compounds or the elemental metal would exert an opposite effect, easing carrier transfer between planes.

Any or all of these mechanisms (among other) might be occurring in the metal-doped pyro-polymers. It is hoped that this study, in conjunction with previous ones, might help to elucidate this situation, as well as extend the available data on the electrical properties of this class of materials.

EXPERIMENTAL PROCEDURES

1. Preparation of the Doped Pyro-Polymers

A. Pre-Treatment of Resin

The ion exchange resin (Rohm & Haas XE89, a poly-acrylic acid crosslinked with 6% divinylbenzene) was first washed with HCl to remove any traces of iron which might be present in the material as supplied. Two liters of the resin

(measured under the HCl solution) were slurried with two liters of 1-N HCl (reagent grade and distilled water) in a 4-l beaker and left standing for four hours. The slurry was then poured into a 2-in. diameter glass column with a stopcock at the bottom. A wad of glass wool prevented the resin from draining out of the column when the stopcock was opened. The resin was washed with an additional 3 liters of 1-N HCl at a rate of about 1/4 liter/hour.

The acid was followed by a washing with 6 liters of distilled water over a period of 3 hours until a pH of approximately 6 was attained. There was a noticeable increase in the volume of the resin as the acid was removed. At all times, the liquid level was maintained above the resin to prevent channeling.

The slurry was then poured into a beaker and enough 28% reagent grade NH_3 was added, with continuous stirring, to bring the pH to 10. Small amounts of NH_3 solution had to be added over a 3 hr. period to maintain the pH as NH_3 was absorbed. The resin underwent a pronounced swelling upon addition of the NH_3 , roughly doubling its original volume. This swelling is reported to increase the speed and thoroughness of the doping procedure^{1,2}. The resin- NH_3 slurry was left standing, with occasional stirring, for 57 hrs., after which it was poured back into the column (in two installments), and washed with a total of 30 liters of distilled water to bring the effluent pH to approximately 7.

B. Doping

Three hundred ml. (measured under water) of the resin were placed in each of twelve 500 ml. bottles, allowed to settle, and the excess water decanted. To each bottle was added 100 ml. of a solution of either Na, Ca or Th nitrate of the concentration indicated in

Table I. The slurry was rapidly stirred with a TFE-glass, motor-driven paddle as the solutions were added.

TABLE I - Doping Concentration

Code	I	II	III	IV
(metal ion conc.)	4.5N	1.5N	0.45N	0.15N

The remaining resin (approx. 500 ml.) was left in the NH_4 form.

When the solutions of $\text{Th}(\text{NO}_3)_4$ were added to the resin, a thick, white, gelatinous precipitate formed. Adding some NH_4OH to a separate solution of $\text{Th}(\text{NO}_3)_4$ indicated this precipitate was thorium hydroxide, formed as the Th^{4+} ions replaced the NH_4^+ in the exchange reaction. Enough HNO_3 was added to the jars to bring the pH to approximately 3, dissolving the precipitates. Unfortunately, this decreased the amount of Th absorbed by the resin, resulting in low doping levels in the final pyro-polymers. No precipitates were formed with the Na^+ and Ca^{++} solutions. The jars were left standing with frequent shaking for 20 days to allow the ions to be evenly absorbed throughout the resin.

After the 20 days period, the contents of each jar was dumped into the column and washed with distilled water to remove any unabsorbed ions which might leave a salt residue in the final polymer. Six liters of water were used for Ca^{++} I, Na^+ I and the entire Th^{4+} series (to remove the added HNO_3), and 3 liters for the remaining samples.

Each sample was then placed in an evaporating dish and dried overnight in a forced-air oven at 100°C . The dried products occupied only a fraction of their former volume, but were still in a white, spherical form.

C. Pre-oxidation

The dried, doped resin was then placed in a petri dish and pre-oxidized at 300°C. for 24 hours. It has been shown that this procedure decreases the weight loss in the subsequent pyrolysis operation, probably by allowing the hydrogen in the sample to be driven off as water rather than as hydrocarbons during pyrolysis⁹. The pre-oxidation also cross-links the resin, the importance of which will be described below.

Sodium and calcium imparted an appreciable degree of oxidation resistance to the resin. After 24 hours at 300°C. the Na⁺I sample was a deep purple, while the Ca⁺⁺I was light brown. All the other samples were black, at least on the surface. After much difficulty with the subsequent pyrolysis procedure, in which "foaming" occurred if pre-oxidation had been insufficient, it was discovered (by grinding them in a mortar) that in some cases, although black on the surface, the resin spheres had not been completely oxidized throughout. When this occurred, it was necessary to grind the complete sample in the mortar, and return it to the oven for further oxidation.

D. Pyrolysis

After oxidation, the samples were pyrolyzed at 600°C. to drive off the major portion of the volatiles and minimize the porosity of the final pellet. Approximately 7 grams of oxidized resin were placed in the covered combustion boat and slid into the furnace tube. Helium was passed through the tube into a benzene-filled bubbler at a low rate (roughly 2--3CC/min.). When the sample reached 400°C., a rapid evolution of gas began, which was trapped in the bubbler and the cool end of the tube as a brown foul-smelling tar.

The temperature was maintained at 600°C. for two hours, after which the current was shut off and the sample allowed to cool. The helium atmosphere was maintained until the sample had cooled down at least to 100°C.

A great deal of trouble was encountered during the pyrolysis of samples which were later found to be incompletely oxidized. These materials "foamed" leaving the boat and plugging the "down-wind" part of the tube. In most of these instances, very little resin was left in the boat. After a thorough pre-oxidation, however, the resin retained its granular form and remained in the boat, with some shrinkage and a very slight cohesion.

E. Molding Pellets

The product of the 600°C. pyrolysis was ground in a mortar with 20% Bakelite BRP 5417, a low-ash phenolic binder, which had been previously dried for 24 hours at 100°C.

Approximately 0.6 g. of the above material was molded to a hard, crosslinked pellet cured for 15 minutes at 32,000 psi, with the press platens maintained at 325°F. (The heavily doped Th materials had a higher density than the others, and 0.8 g. was used to mold the Th⁴⁺ I samples.) Upon the removal from the mold, the pellets were placed in an airtight glass vial.

The more highly doped samples formed an extremely strong bond with the steel mold surfaces in spite of attempts to prevent sticking by meticulously polishing the mold surfaces. The bond formed with the Na⁺ I samples was the strongest, but those formed by the Na⁺ II and the highly doped Ca¹⁺ and Th⁴⁺ samples were by no means weak - in most cases large chunks of cured resin were left sticking to the mold when the pellets were forcibly removed.

The problem was finally solved by very lightly brushing the hot mold surfaces with a TFE dispersion, "Waxlube Liquid Teflon" (Bel-Art Products, Pequannock, N. J.), cut 4:1 with distilled water and containing a few drops of triethylamine as a suspending agent. A fresh coat of this mold-release agent had to be applied for each pellet, as most of the TFE remained on the surface of the pellet.

F. Heat Treatment

The surfaces of each pellet were carefully sanded with aluminum oxide cloth, 320 grit, to remove all traces of TFE. A camel's hair brush was used to remove any loose surface material from the pellets. Their weights were then recorded and four (I, II, III, IV of a given ion) were placed side-by-side in the graphite boat (their positions carefully noted), and were covered by a graphite retaining spool to hold them in place. The pellets were arranged with their long axes parallel to the axis of the tube and boat, and placed so that their centers would be near the junction of the regulating thermocouple when the boat was inserted in the tube. The pellets were maintained at the desired temperature (800, 1000, or 1200°C.) for two hours with helium passing over them as in the 600° pyrolysis. After they had cooled, the boat was removed to the dry-box (the samples were kept isolated from the atmosphere until the electrical measurements were completed), and the pellets were then placed in individual, screw-top bottles which had been kept in the dry-box during the heat treatment.

G. Electrical Measurements

The sample was removed from its bottle and placed in the cell, which was then inserted in the brass box and sealed by tightly bolting on the cover, all work being done in the dry-box. (The cell,

its box and cover were kept in the dry-box for at least two hours prior to inserting the sample). The enclosed sample was then removed from the dry-box and placed between the poles of the large magnet with dried N_2 passing through the copper box. All leads were connected and at least a half hour allowed to reach temperature equilibrium.

The thermocouple EMF was then read, and with a current of 10 milliamps flowing through the sample, the voltage drops between the two sets of resistance contacts (see Figure 1) were read and recorded. This procedure was repeated at least three times to insure reproducibility.

The current through the sample was then increased to roughly 100 milliamps, and the magnet current (which varied between 8 and 12 amps) was turned on. The Hall voltage, the magnet current, and the sample currents were recorded. The magnet current was then reversed as quickly as possible and the Hall voltage again recorded. This procedure was repeated several times, with the initial direction of the field alternated (to counteract any effects the magnet's field might have on the galvanometer). The magnet current readings were recorded between each reversal of field, since the magnet current decreased slowly due to the heavy drain on the batteries. The direction of the magnetic field and the sign of the potentiometer setting were recorded at each reading to determine the sign of the Hall voltage. This method had the advantage of giving a reading of twice the Hall voltage (the difference between the field-reversed readings), which is important in view of the small Hall voltages encountered.

The field strength-current calibration for the Hall magnet was obtained with a previously calibrated sample in place of the test pellet.

The cell-box was then immersed in a Dewar flask containing a stirred dry-ice-acetone slurry. After allowing an hour to reach temperature equilibrium, the resistance was measured exactly as was done at room temperature. The box was taken from the bath and allowed to warm up and the pellet was then removed, weighed, and measured with a micrometer, after which it was replaced in its bottle and stored in a dessicator.

H. Analysis

Samples of the 1000°C. pellets were commercially analyzed for C, H, N, and metal content. Duplicates of each sample were provided, and the results checked to within 6%.

The above analyses were assumed to apply roughly to the 600° and 1200° calcium and thorium-doped pellets also, since the differences in weight loss between pellets pyrolyzed at the three temperatures was slight. In the case of the sodium-doped pellets, however, the strong probability (see Discussion of Results) that metallic sodium distilled from pellets heat treated at 1000° and 1200°C. invalidates such an assumption. Therefore, the variations of electronic properties with sodium doping level are presented only for the 1000°C. pellets actually analyzed. The 800° and 1200° pellets are referred to by the codes for the initial doping ion concentrations (Table 1).

APPARATUS

Pre-oxidation

The doped resins were pre-oxidized in a Cooley type MP2 electrically heated muffle furnace, with an internal cavity approximately 6 x 4 x 13-1/2. The temperature was automatically controlled to within $\pm 10^{\circ}\text{C}$.

Pyrolysis & Heat Treatment

Heating at 600, 800, 1000 and 1200 $^{\circ}\text{C}$. was done in a Sentry model V, size 2 electric furnace. The furnace temperature was controlled to within $\pm 5^{\circ}\text{C}$. by a Leeds & Northrup "Micromax" model R controller.

The pellets were placed side-by-side in a semi-cylindrical graphite boat 6 in. long x 1 in. OD x 1/2 in. ID, with their long axes parallel to that of the boat, and were held in place with a graphite spool. Temperature variation among pellets side-by-side was thus minimal and probably did not exceed 2 $^{\circ}\text{C}$.

The boat and charge were placed in a 1 in. stainless steel pipe passing through the furnace, with the center of the charge as near as possible to the junction of the controlling thermocouple. One end of the stainless steel pipe was connected to the helium supply and the other was screwed into the side of the dry-box.

Molding

The pellets were molded in a three-piece semi-positive hand mold with a 1" x 1/4" x 0.08" min. cavity and a Preco model PA6 press with electrically heated platens.

Measurement Cell

All the electrical contacts in the measurement cell (Figure 1) were either made of platinum foil, or were platinum-plated for good electrical contact.

The cell was placed in a sheet brass box closed by a 1/8" brass top and rubber gasket. Two pieces of 1/4" OD copper tubing were soldered through the top, one for the exit of the electrical leads and the other for nitrogen inlet.

Electrical Equipment

The resistivity, Hall and thermocouple leads were all fed to a Leeds & Northrup type K-3 potentiometer through a double-pole 4-throw wafer switch. See Figure 2. The current flowing through the sample was regulated with a Heathkit RD-1 resistance decade box and measured with a milliammeter. Its direction could be reversed with a DPDT switch. Power was supplied by a six-volt storage battery. The large Hall magnet had two 1153-turn coils, and drew up to 13 amps from a series of six twelve-volt storage batteries.

Qualitative thermoelectric power measurements were made using two alligator clips connected to a millivolt meter, one end of the sample being heated with a small soldering iron.

X-Ray Spectrographs

X-ray spectrographs were made with a Norelco geiger-counter X-ray spectrometer, type No. 12021, using an iron (α -line) source filtered by a thin Mn window.

Calculations

1. Resistivity

$$\rho = R \frac{wt}{d}$$

where

ρ = resistivity, ohm-cm

R = resistance of sample between potential probes,
ohms

w = width of sample, cm

t = thickness of sample, cm

d = distance between potential probes, cm

In terms of the experimentally measured quantities, with a current of 10 milliamperes flowing through the sample, and potential probes 1.675 cm apart, this becomes

$$\rho = 385 Ewt$$

where

ρ = resistivity, ohm-cm

E = potential drop between probes, volts

w = sample width, inches

t = sample thickness, inches

Estimate of the maximum instrumental error in resistivity measurements.

$$\rho = \frac{Ewt}{I d}$$

where

I = current through sample, amperes

The errors in each individual factor are estimated as follows:

E = .001 \pm .0000001 volts

w = .24 \pm .001 inches

t = .1 \pm .001 inches

$$d = 1.675 \pm .05 \text{ cm}$$

$$i = 0.01 \pm .0002 \text{ amperes}$$

$$\frac{\Delta \rho}{\rho} = \frac{\Delta E}{E} + \frac{\Delta i}{i} + \frac{\Delta W}{W} + \frac{\Delta t}{t} + \frac{\Delta d}{d}$$

$$= \frac{.0001}{.0000001} + \frac{.0002}{.01} + \frac{.001}{.24} + \frac{.001}{.1} + \frac{.05}{1.675} = .06 \text{ or } 6\%$$

2. Hall Coefficient

The Hall voltage was given by¹⁰

$$V = 10^{-8} \frac{R_H I H}{t}$$

where

I = current flowing through sample, amperes

H = magnetic field strength, Gauss

t = thickness of sample (perpendicular to potential probes), cm

V = Hall voltage, volts

R_H = Hall coefficient, cm³/coulomb

The Hall coefficient then becomes, in terms of the experimentally measured quantities

$$R_H = 2.54 \times 10^8 \frac{Vt}{IH}$$

where

R_H = Hall Coefficient, cm³/coulomb

V = Hall voltage, volts

t = thickness of sample, inches

i = current through sample, milliamps

H = magnetic field strength, kilogauss

3. Energy Gap

Since the materials investigated here are degenerate semi-conductors (i.e., they have a large number of carriers and a small energy gap), the usual application of Boltzmann statistics to determine the energy gap ($2kT \times$ slope of a $\log \sigma$ vs. $1/T$ plot) is not strictly valid.

Energy gaps were calculated by applying Fermi-Dirac statistics to a degenerate, intrinsic model as follows:

$$a. \quad \sigma = n\mu/|e|$$

where

σ = conductivity, $(\text{ohm-cm})^{-1}$

n = number of carriers per cc

$\mu = \frac{\mu_e + \mu_n}{2}$ = average mobility of holes and electrons, $\text{cm}^2/\text{volt-sec.}$

$|e|$ = carrier charge, coulombs

Since n is proportional to $T^{3/2} F_{1/2}(\eta^*)$ ¹¹ and μ is approximately proportional to $T^{-3/2}$,¹² if the effective masses are assumed equal, σ is therefore proportional to $F_{1/2}(\eta^*)$

where

$F_{1/2}(\eta^*)$ = Fermi function

$\eta^* = E_G/2kT$

E_G = energy gap

k = Boltzmann constant

T = absolute temperature

b. Values of $F_{1/2}(\eta^*)$ as tabulated by McDougall and Stoner¹³ were plotted vs. η^*

c. Values of $\frac{\sigma}{T^{3/2}}$ vs. η^* were plotted against E_G .

where

ρ_1 = resistivity at $T_1 = -70^\circ\text{C}$

ρ_2 = resistivity at $T_2 = 20^\circ\text{C}$

Where measurement temperatures differed from T_1 and T_2 , short extrapolations to these temperatures were made with a $\log \rho$ vs. $1/T$ plot, but in most cases, since the temperature varied less than 5°C from T_1 or T_2 , and the change in resistivity with temperature was so small, this made little difference.

d. Energy gaps were obtained from the above plot using calculated values of ρ_1/ρ_2 .

4. Resistivity-Density Corrections

Corrections of the measured resistivities for small variations in pellet density were based on the assumption that the conductivity is directly proportional to the density, i.e.,

$$\rho_c = \frac{d_o}{d_c} \rho_o$$

where

ρ_c = corrected resistivity

ρ_o = observed resistivity

d_c = corrected density

d_o = observed density

The corrected densities were estimated by using the mixture law¹⁴, $v = w_1V_1 + w_2V_2$,

where

v = specific volume of mixture = $1/d_c$

V_1 & V_2 = specific volumes of components 1 & 2

w_1 & w_2 = weight fractions of components 1 & 2

If only carbon (graphite) and the doping metal are assumed present, (1) $w_1 = (1 - w_2)$, and (2) $v = V_1 + w_2(V_2 - V_1)$, with sub-

script 1 signifying graphite and 2 the doping metal. To account for the porosity of the pellets, equation (2) was modified to

$$v = v_0 + w_2(v_2 - v_1) \quad (3)$$

where

v_0 = specific volume of the undoped pellet

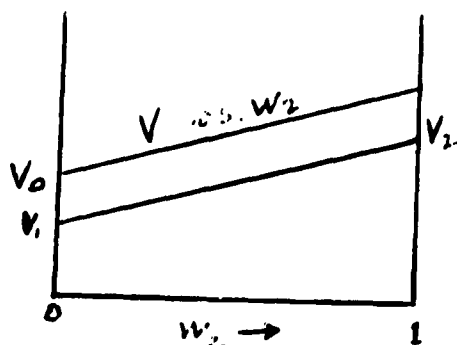
The procedure is shown diagrammatically below. The following values were used¹⁵:

(graphite) = 2.25 g/cc

(calcium) = 1.54

(thorium) = 11.5

(sodium) = 0.971



5. Analyses

Sample analyses for Ca and Th were reported as weight per cent C, H, N and mg ash. These were converted to atom per cent using the following assumptions:

- a. The ash reported was either CaO or ThO₂
- b. The balance of the sample weight was oxygen.

Sodium content was reported directly in weight per cent, and assumption (b) was applied.

The results are given in Table 2.

Table 2. - Sample Analyses

Averages of duplicate analyses of samples pyrolyzed at 1000°C.,
in atom percent.

	<u>Metal</u>	<u>Code</u>	<u>C</u>	<u>H</u>	<u>N</u>	<u>O</u>
Ca	9.33	I	41.4	24.2	0.74	24.2
	5.05	II	63.8	16.3	1.46	13.5
	2.36	III	85.4	6.65	1.58	3.95
	1.06	IV	89.3	5.21	2.15	2.21
Th	2.81	II	71.2	14.2	1.17	11.9
	2.63	I	73.7	12.7	0.622	10.3
	0.775	III	82.7	9.86	1.75	5.00
	0.322	IV	84.5	9.23	1.99	3.92
Na	2.38	I	75.4	14.6	0.33	7.33
	2.36	II	70.7	18.2	2.0	6.78
	1.86	III	75.4	11.8	2.1	8.76
	1.43	IV	82.6	11.5	2.1	2.45
	0	NH ₄	87.8	5.5	.5	6.2

Pyrolyzed @ 800°C.

Na	11.83	I	53.67	12.69	5.52	16.29
	7.20	II	59.61	14.28	4.08	14.81
	6.20	III	66.19	11.44	3.27	12.90
	1.90	IV	70.32	16.83	2.04	8.93

DISCUSSION OF RESULTS

Weight Losses

The weight losses of pellets pyrolyzed at 800°, 1000° and 1200°C. are presented in Table 3. As might be expected, the losses increase with pyrolysis temperature. The major portion of the volatiles are driven off below 1000°C., with only a slight loss in weight between 1000° and 1200°C.

The calcium-doped samples show an increase in weight loss with doping level, while the weight loss decreases with increasing thorium content. Sodium-doped pellets pyrolyzed at 800°C. appear to undergo a slight initial decrease in weight loss, followed by a larger increase as the doping level is raised. At 1000°C. and 1200°C., however, the weight losses increase with sodium content.

The behavior of the sodium-containing pellets might be explained by the fact that metallic sodium boils at 880°C.¹⁶ If, during the pre-oxidation, the sodium is converted to Na₂O, which is subsequently reduced by the abundant carbon in the pellets, metallic sodium could simply distill from the pellets during heat treatment at 1000°C. and 1200°C.

Other evidence for this possibility is the fact that the analyses of the 1000° sodium pellets show a much smaller variation in doping level than would be expected from the original ion concentrations and volume variations observed in the doped resin. Also, the initially highly doped pellets exhibited a very low density (Table 4), blistered appearance and weakness when pyrolyzed at 1000° and 1200°C. Such a distillation of the doping metal, however, would not explain the high weight loss in a sodium-doped pellet pyrolyzed at 800°C., nor would it account for the behavior of the

Table 3. - Weight Losses

<u>Atom %</u>	<u>Code</u>	<u>Pyrolysis Temperature</u>		
		<u>800°</u>	<u>1000°</u>	<u>1200°</u>
0 Ca	NH ₄	19.8%	23.8%	26.2%
1.06	IV	21.6	26.9	29.3
2.36	III	25.0	30.6	32.6
5.05	II	29.7	33.1	33.5
9.33	I	36.6	40.4	40.0
0 Th	NH ₄	19.8	23.8	26.2
0.322	IV	19.6	23.7	23.4
0.775	III	18.4	21.6	22.4
2.63	I	15.6	18.5	19.5
2.81	II	14.5	16.0	16.5
0 Na*	NH ₄	19.8	23.8	26.2
1.43	IV	19.4	26.6	31.4
1.86	III	17.8	27.3	33.0
2.36	II	28.8	40.5	47.3
2.38	I	--	62.6	64.8

* Valid only for 1000° samples actually analyzed.

calcium-doped pellets since calcium does not boil until 1240°C.¹⁷

It is possible that sodium and calcium catalyze the reactions which lead to weight loss.

Resistivity

The room-temperature (20°C.) resistivities of the pellets as a function of pyrolysis temperature are shown in Figure 3. In all cases, the curves are quantitatively similar, the resistivities showing a large drop between 800° and 1000°C. and leveling off above 1000°C. This correlates with the observation that the major portion of the weight loss in pyrolysis occurs below 1000°, indicating that the materials undergo major structural changes in the 800° to 1000° temperature range.

Below 800°, the pellets evidently contain fairly large amounts of H, N and O. As the pyrolysis temperature is raised these elements are driven off as volatile gases (H₂O, CO, CO₂, NH₃, CH₄, and higher hydrocarbons, etc.), as the remaining material begins to condense into small crystallites. The loss of volatiles would be expected to produce free radicals at the edges of the crystallites, which in turn create carriers (see equation 1, Introduction). As the pyrolysis temperature is raised, more carriers are produced by the dissociation of carbon atoms in the crystallite interiors (equation 2, Introduction). The size of the crystallites also increases with the pyrolysis temperature. Since it has been shown that graphitic structures (as those crystallites are presumed to have) are relatively good conductors along their planar dimensions ($\rho = 10^{-3}$ to 10^{-5} ohm-cm)⁸, increasing these dimensions logically increases the overall conductivity of the material.

Sodium doping appears to make the resistivity less temperature sensitive. At 800°C., the resistivities of the sodium-doped samples are lower than that of the undoped pyro-polymer, while at 1000° and 1200°, they are higher.

Data for the undoped pyro-polymers agree fairly well with previous results^{1,2,5,18}.

The peculiar variations of resistivity with doping level are illustrated in Figure 4. In the case of the calcium-doped specimens, the resistivity is first seen to decrease slightly, followed by a large increase, another slight decrease and then a gradual rise as the calcium content is increased. Addition of thorium initially increases the resistivity, which then slowly drops and levels off at a value below that of the undoped polymer.

The shapes of any one of these curves, particularly those for the calcium-doped samples, would ordinarily be ascribed to experimental error or other random variation. However, the similarity in the shapes of curves obtained independently at the three different pyrolysis temperatures (they practically could be superimposed by translation along the resistivity axis) precludes such an explanation. In addition, behavior qualitatively similar to that observed in the thorium-doped materials was previously reported for nickel-doped polymers pyrolyzed at 1000° and 1200°C.¹ In the latter case it was attributed to an increase in electron scattering due to distortion of the crystallite lattice by the doping metal¹.

If the shapes of these curves is to be attributed, at least in part, to factors other than the doping level, these factors must have contributed their effects in the preparation of the samples, since each pellet of a given doping level, although indivi-

dually molded and pyrolyzed, came from the same batch of molding powder. A comparison of the resistivities and pellet densities provides a possible clue (see Table 3).

If all other factors were held constant, the densities of the pellets would be expected to vary as a smooth function of the doping level. Such is not the case for these pellets. In many instances, high resistivities are seen to correspond to low pellet densities, and vice-versa. This suggests a resistivity-void space effect similar to that used in telephone mouthpieces and microphones. These density variations are definitely not the only cause of variations in resistivity with doping level, however, since the resistivities are by no means smooth functions of the pellet densities. These density variations probably arise from differences in particle size in the original molding powder. Slight variations in the molding cycle probably contribute some small random variations, also.

An attempt has been made to correct the resistivity values for density variations, based on the assumption that resistivity is inversely proportional to the pellet density. Details of the procedure are given in the Calculations section. The corrected resistivity-doping level curves are shown in Figure 5. As may be shown by comparing Figures 4 and 5, and Table 4, this correction does not drastically alter the shapes of the curves, but it does minimize the initial rise and eliminate the second dip in the data for the calcium-doped samples.

The doping metals may be assumed to exist in one (or more) of four possible states in the pyro-polymers: (1) as clusters of the free metal, as is thought to be at least partially the case

Table 4

Atom % Ca	Code	Pyrol. Temp.	ρ , measured	d, measured	d, calcul.	ρ , corr.
0%	NH ₄	800°C.	.0598 Ω -cm	1.24 g/cc	1.24 g/cc	.0598 Ω -cm
1.06	IV		.0530	1.31	1.23	.564
2.36	III		.0975	1.19	1.22	.0950
5.05	II		.0956	1.34	1.19	.108
9.33	I		.113	1.14	1.15	.112
0	NH ₄	1000°	.0109	1.27	1.27	.0109
1.06	IV		.00931	1.33	1.26	.00983
2.36	III		.0149	1.21	1.25	.0139
5.05	II		.0142	1.36	1.22	.0158
9.33	I		.0244	1.14	1.18	.0236
0	NH ₄	1200°	.00914	1.28	1.28	.0914
1.06	IV		.00745	1.29	1.27	.00756
2.36	III		.0124	1.14	1.25	.0113
5.05	II		.0111	1.33	1.23	-.120
9.33	I		.0159	1.15	1.17	.0154
0	NH ₄	800°	.0598 Ω -cm	1.24	1.24	.0598 ohm-cm
.322	IV		.1048	1.22	1.28	.100
.775	III		.0989	1.34	1.31	.101
2.63	I		.0497	1.98	1.46	.0674
2.81	II		.0753	1.94	1.48	.0986
0	NH ₄	1000°	.0109	1.27	1.27	.0109
.322	IV		.0168	1.26	1.30	.0163
.775	III		.0137	1.39	1.35	.0141
2.63	I		.00998	2.01	1.50	.0134
2.81	II		.00984	1.96	1.52	.0127
0	NH ₄	1200°	.00914	1.28	1.28	.0914
.322	IV		.0126	1.23	1.31	.0118
.775	III		.0114	1.38	1.36	.0116
2.63	I		.00783	2.00	1.52	.0103
2.81	II		.00814	1.90	1.53	.0101

Table 4 (Continued)

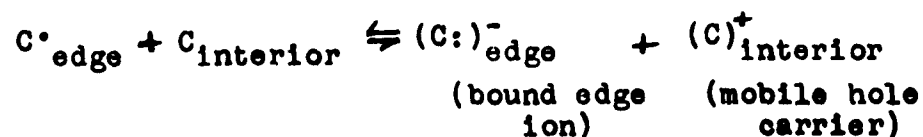
In order of decreasing doping level

Atom % Na	Code	Pyrol. Temp.	ρ , measured $\Omega\text{-cm.}$	d, measured g/cm^3	d, calcul. g/cm^3	ρ , corr. $\Omega\text{-cm.}$
	I	800°	--	--		
	II		.0387	1.30		
	III		.0330	1.33		
	IV		.0331	1.34		
2.38	I	1000°	.0205	.727	1.22	.0122
2.36	II		.0167	1.10	1.22	.0151
1.86	III		.0114	1.28	1.24	.0118
1.43	IV		.0117	1.23	1.24	.0116
	I	1200°	.0149	.0739		
	II		.0134	1.01		
	III		.0984	1.20		
	IV		.0979	1.21		

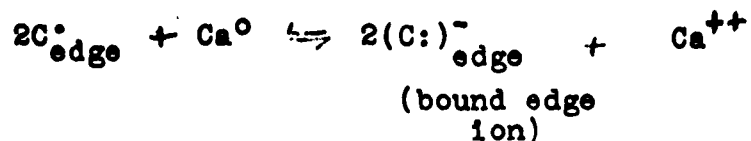
for nickel-doped pyro-polymers¹, (2) as oxides (Na_2O , CaO , ThO_2), (3) as carbides (Na_2C_2 , CaC_2 , ThC_2)¹⁹, or (4) as metal bonded in the carbon lattice. Forms (2) and (3) would be expected to be non-conductors in the solid state²⁰. On this basis, increased resistivity could be ascribed to clusters of non-conducting oxides or carbides hindering carrier transfer between crystallites and the stacked sheets of the crystallites. Clusters of free metal would be expected to produce the opposite effect. Metal bound in the lattice of the aromatic carbon sheets might increase resistivity by generating hole carriers, or decrease it by causing additional electron scattering.

In the case of calcium, the presence of calcium oxide, formed in the pre-oxidation step, is a distinct possibility. Analyses show (Table 2) oxygen to be present in excess of the stoichiometric amount needed for the oxide, although the O/Ca ratio is not constant. The formation of calcium carbide, through the reaction¹⁹ $\text{CaO} + 3\text{C} \longrightarrow \text{CO} + \text{CaC}_2$ also cannot be ruled out, in view of the large excess of carbon present. Similar possibilities exist for other metals.

Another mechanism through which doping might influence the resistivities of pyro-polymers is by donation of electrons to the system (if the free metal can be assumed to be present at some time during the formation of the pyro-polymers). As was discussed in the introduction, the loss of small molecules is thought to leave free radicals at the crystallite edges, which in turn create holes



In the presence of a metal, whose outer electrons are much more loosely bound than are those of carbon, the following type of reaction seems entirely logical (using calcium as an example):



The above reaction, in effect, uses up holes which would otherwise contribute to conduction in the undoped material. In non-degenerate semi-conductors, where the product of the number of positive and negative carriers is always the same²⁵, the reaction would result in a corresponding increase in the number of electrons. For degenerate semi-conductors (as these materials are), however, it has been shown that the carrier product is not constant²², since the maximum possible number of carriers (limited ultimately by the atoms of material present) is being approached. Thus, doping of a degenerate semi-conductor could decrease the number of carriers through this mechanism, thereby increasing the resistivity. It is conceivable that the metal ions might contribute some ionic conduction, but their mobilities in the solid state would be extremely low compared to those of electrons and holes, and they would contribute little to the overall conduction.

Reproducibility of resistivity measurements on a given sample was within 0.1%, and between duplicate samples at 1000° and 1200° (where the resistivity-pyrolysis temperature coefficient is small) within 5%. A slightly greater deviation (10-15%) for 800° samples is felt to arise from slight variations in the pyrolysis temperature, rather than the measurement procedure, since the drop of resistivity with pyrolysis temperature is relatively great in

this temperature range. A quantitative estimate (see Calculations) shows that the error in measurement is probably less than 6%.

Energy Gap

The variation in energy gaps with temperature is shown in Figure 6. As might be expected, the data show greater scatter than the resistivity-pyrolysis temperature plots, since each value of energy gap involves two independent measurements of resistivity and temperature. Nevertheless, the energy gaps are seen to decrease with pyrolysis temperature, but a comparison with Figure 3 shows that the decrease is less than that of resistivity with temperature. In terms of the band theory, this indicates that raising the pyrolysis temperature decreases resistivity partially by increasing the number of carriers through a lowering of the energy gap, but that higher carrier mobilities must also contribute to the decrease. This will later be treated in a more quantitative manner. The latter effect probably arises from the increase in size of the crystallites with pyrolysis temperature, allowing carrier to progress with fewer "jumps" between crystallites.

In general, increasing the doping level is seen (Figure 7) to cause an initial rise in the energy gap. The gap appears to level off at higher impurity concentrations. This rise in energy gap is consistent with the previously discussed effect doping metals may play in lowering the carrier density.

Hall Coefficient

Measurement of the Hall coefficients of the pyro-polymers was extremely difficult, largely because of the low Hall voltages encountered (in the range of 1 to 10 microvolts). The many pitfalls in the measurement of Hall coefficients, such as contact potentials, heterogeneity of specimens, thermal effects, etc. have

been elaborated upon in the literature^{8,21}. It is hoped that they were minimized by platinum-plated contacts, low currents, reversal of the magnetic field and current flow (giving potential differences of twice the actual Hall Voltage), and by averaging a fairly large number (6-10) of individual determinations on each sample. The individual determinations were usually reproducible to within 25-30%.

Perhaps the most significant result of the Hall coefficient determinations is the fact that, without exception, the coefficients are negative. Since this result conflicts with most of those observed for nickel- and aluminum-doped pyro-polymers^{1,2}, it was verified in four ways, (1) by tracing the electrical measurement circuits, by calibrating the apparatus with (2) a known piece of n-type germanium and (3) a directly synthesized p-type organic semi-conductor prepared by E.H. Engelhardt, and (4) by qualitative Seebeck coefficient measurements.

Figure 8 presents the Hall coefficients as a function of pyrolysis temperature. They appear to decrease (i.e., become negatively larger) as the pyrolysis temperature is raised, although there is some indication (dotted lines) that they may, in certain instances, rise slightly to a maximum near 1000° before decreasing.

The Hall coefficient shows a decrease (becomes negatively larger) as the calcium and thorium doping levels are raised (Figure 9). Although the decrease is greater for the calcium-doped samples, their doping levels are approximately three times higher than those achieved with thorium. The slopes, therefore, are roughly comparable.

These Hall coefficients are similar in sign and magnitude to that of natural graphite⁸. Klein has recently interpreted

the Hall coefficient as a measure of morphological perfection in terms of crystalline size and rotational order. Unfortunately, according to his work with pyrolytic graphites, such coefficients should be typical of highly ordered structures⁸, a description which these pyro-polymers do not fit. There is some indication, however, that negative Hall coefficients may be observed for soft carbons in a range of pyrolysis temperatures investigated here⁸. Hennig has also prepared graphites with similar Hall coefficients^{23,24}. The coefficients observed here agree well in sign and magnitude to those observed for undoped 1000° and 1200° pyro-polymers in the investigation of nickel-doped materials¹.

Thermoelectric Power (Seebeck Coefficient)

Qualitative thermoelectric power measurements were made to provide an independent check on the sign of the dominant carrier in the pyro-polymers. In all cases, the hot end of the pellet was positive, indicating n-type conduction.

X-Ray Spectrographs

An X-ray spectrograph (Figure 10) of the undoped pellet pyrolyzed at 1200° showed the specimen to be almost amorphous or to be microcrystalline. Two very broad maxima were observed at $2\theta = 31^\circ$ and 55° , using $\text{Fe}^- \alpha$ radiation. The former peak corresponds to a spacing of approximately 3.5 Angstroms, the distance between layers in the graphite structure⁸. The most highly doped thorium sample (only 2.8 atom %) had a similar spectrum, indicating that the metal was distributed throughout the carbon structure in a manner which does not produce any significant crystallinity. On the other hand, the highly doped sodium (2.4 atom %) and calcium (9.3 atom %) polymers showed sharp peaks, implying the presence of the metals in clusters of crystalline material. The broad maxima

at $2\theta = 31^\circ$ and 55° were also eliminated in these samples. The least highly doped calcium sample (1.1 atom %) had a spectrum similar to that of the undoped material, with a few very small peaks.

The above results provide a possible explanation for the variation in resistivity of the calcium-doped pyro-polymers with doping level. They indicate that calcium is present in different forms and affects the polymer structure in a different manner at high and low doping levels.

At the lowest doping level, where the resistivity is observed to decrease slightly from that of the undoped material, the presence of the calcium does not appear to contribute much (if any) crystalline material, and does not distort the basic structure of the undoped pyro-polymer. At these low concentrations, then, the calcium may exist in the basic carbon crystallite lattice, creating additional hole carriers in a manner similar to that in which doping with a trivalent metal does in germanium or silicon. Beyond a certain level, however, additional calcium can no longer be accommodated in the crystallite lattice structure, and it then concentrates in crystalline oxide or carbide clusters between the crystallites and the aromatic layers, causing the observed disappearance of the 2θ - 31° maximum by a distortion of the normal graphite layer spacing in the crystallites.

Thorium, which does not appear to alter the structure of the undoped material at the doping levels achieved, could also take its place among the carbon atoms in the crystallite lattice, but since it is tetravalent like carbon, would produce no holes. Thus, the initial rise in resistivity with thorium doping could result from the scattering mechanism previously postulated.

Sodium almost certainly would be found either as an oxide or carbide, or bound to the crystallite edges due to its high reactivity, any or all of which would produce the observed resistivity increase at 1000° and 1200°C.

Estimation of Carrier Densities and Mobilities

The carrier densities and mobilities in these pyro-polymers may be estimated from typical data for the materials. Both intrinsic and single-carrier models will be used, since these materials are probably somewhere in between these two extremes.

For a degenerate semi-conductor,

$$\sigma = |e| (n_e \mu_e + n_h \mu_h) = |e| (c n_e + n_h) \mu_h$$

$$R_H = \frac{-(n_e \mu_e^2 - n_h \mu_h^2)}{|e| (n_e \mu_e + n_h \mu_h)^2} = \frac{-(n_e c^2 - n_h)}{|e| (n_e c + n_h)^2}$$

where

- σ = conductivity, (ohm-cm)⁻¹ = 1/ρ
- |e| = carrier charge, coulombs
- n_e = number of electrons per cm³
- n_h = number of holes per cm³
- μ_e = electron mobility, cm²/volt-sec.
- μ_h = hole mobility, cm²/volt-sec.
- c = μ_e/μ_h = mobility ratio
- R_H = Hall coefficient, cm³/coulomb

At 1200°C, typical data for the pyro-polymers are:

$$R_H = -2 \times 10^{-2} \text{ cm}^3/\text{coul.}$$

$$\sigma = 1 \times 10^2 \text{ (ohm-cm)}^{-1}$$

For a single carrier model, n_h = 0, and the above equations reduce to:

$$n_e = \frac{-1}{|e| R_H} \quad ; \quad \& \quad \mu_e = \frac{\sigma}{|e| n_e}$$

which give the following results:

$$n_e = \frac{-1}{(1.6 \times 10^{-19})(-2 \times 10^{-2})} = 3 \times 10^{20} \text{ cm}^{-3}$$

$$\mu_e = \frac{10^2}{(1.6 \times 10^{-19})(3 \times 10^{20})} = 2 \frac{\text{cm}^2}{\text{v-sec.}}$$

For an intrinsic model, $n_e = n_h$. The mobility ratio will be estimated as $c = 2$, from previous work with nickel-doped pyro-polymers²⁶. The equations then become:

$$n_h = n_e = \frac{-1}{|e| R_H} \quad ; \quad \& \quad \mu_h = \sigma R_H \quad ; \quad \mu_e = 2 \mu_h$$

and

$$n_e = \frac{-1}{3(1.6 \times 10^{-19})(-2 \times 10^{-2})} = 1.6 \times 10^{20} \text{ cm}^{-3}$$

$$\mu_h = \frac{2 \text{ cm}^2}{\text{v-sec.}} \quad ; \quad \mu_e = \frac{4 \text{ cm}^2}{\text{v-sec.}}$$

If the density of a typical pellet is taken as 1.3 g/cm^3 , and it is assumed to be comprised only of carbon, there are

$$\frac{1.3}{12} \times 6 \times 10^{23} \approx 6 \times 10^{22} \frac{\text{carbon atoms}}{\text{cc}}$$

$$\frac{1.4 \times 10^{20}}{6 \times 10^{22}} \approx 2.7 \times 10^{-3} \frac{\text{carriers}}{\text{c atom}}$$

Similar calculations for a typical 800°C pellet, with $R_H = -.01 \text{ cm}^3/\text{coul}$ and $\sigma = 0.17 \text{ (ohm-cm)}^{-1}$ give

$$n = 2 - 6 \times 10^{20} \text{ carriers/cm}^3, \text{ and}$$

$$\mu_e = 0.17 - 0.34 \text{ cm}^2/\text{v-sec.}$$

Thus, calculations based on Hall measurements indicate that increasing the pyrolysis temperature decreases the number of carriers, and that the decreased resistivity is therefore due to an overriding increase in the carrier mobilities.

As was previously noted, E_G measurements indicate that increasing the pyrolysis temperature increases the number of carriers. A quantitative estimate of this effect follows.

It may be shown that for an intrinsic semi-conductor¹¹,

$$n_i = \frac{1}{2\pi^2} \left(\frac{2m_e^* kT}{h} \right)^{3/2} F_{1/2}(\eta^*)$$

where

$F_{1/2}(\eta^*)$ is defined in the Calculations section

m_e^* = effective mass of an electron

n_i = number of electrons (or holes) per cm^3

Assuming the effective mass does not change with pyrolysis temperature,

$$\frac{n_2}{n_1} \approx \frac{F_{1/2}(\eta_2^*)}{F_{1/2}(\eta_1^*)}$$

where subscript 1 signifies the 800°C pyrolysis temperature and 2 the 1000° - 1200° range. Using typical E_G values and the $F_{1/2}(\eta^*)$ data of McDougall and Stoner¹³,

pyrol. temp.	E_G	η^*	$F_{1/2}(\eta^*)$
800°C	.04 ev	-0.79	0.35
1000° - 1200°	.01	- . 2	.58

$$\frac{n_2}{n_1} \approx \frac{0.58}{0.35} = 1.7$$

Therefore, according to energy-gap data, the number of carriers increases roughly by a factor of 1.7 as the pyrolysis temperature is raised from 800°C to 1000° - 1200°C, as contrasted to a two-fold decrease in carrier concentration calculated from Hall measurements.

In view of the relative accuracies of the energy gap and Hall coefficient measurements, calculations based on the former are probably closer to the truth. Also, interpretation of the Hall coefficient in a two-carrier model is not as simple as the preceding equations indicate. In any case, resistivities are seen to decrease by a factor of approximately six or more over the 800° to 1000° - 1200°C range, indicating that the major factor in the decrease over this range is increased carrier mobility, which in turn probably arises from the growth of the stacked aromatic sheets, allowing carriers to progress through the material with fewer "jumps" between sheets.

Using the above band theory equation for n_i , a calculation of the carrier concentration from E_G data may be made, providing a check on the applicability of the band theory to the pyro-polymers.

Assuming $m_e^* =$ rest mass of electron²⁷ = 9.1×10^{-28} g

$\hbar = 1.054 \times 10^{-27}$ erg. sec.

$kT = 0.41 \times 10^{-13}$ ergs.

$F_{\frac{1}{2}}(1)^*$ at 1000° - 1200°C = .58

$$n_i = \frac{1}{2\pi^2} \left[\frac{2 \times 9.1 \times 10^{-28} \times .41 \times 10^{-13}}{(1.054 \times 10^{-27})^2} \right]^{3/2} \times .58$$

$$n_i \approx 1.5 \times 10^{19} \frac{\text{carriers}}{\text{cc}}$$

This result is roughly an order of magnitude smaller than that obtained from resistivity-Hall coefficient data. In view of the many approximations involved in these calculations, the discrepancy is not too great, and may indicate a limited applicability of the band theory to these materials.

An estimate of the effective mass, m_e^* can be had:

If
$$n_e = \frac{-1}{3k/R_H} = 1.0 \times 10^{20} \text{ cm}^{-3}$$

$$\left(\frac{m^*}{m}\right)^{3/2} n_e' = n_e$$

$$n_e' = 1.5 \times 10^{19}$$

$$n_e = 1.0 \times 10^{20}$$

$$\left(\frac{m^*}{m}\right)^{3/2} = \frac{10}{1.5} = 6.667$$

$$\frac{m^*}{m} = \sqrt[3]{44.44} \approx 3.$$

CONCLUSIONS

1. The sodium-, calcium- and thorium-doped pyro-polymers investigated here are degenerate semi-conductors. They exhibit a decrease in resistivity from roughly 0.1 to 0.01 ohm-cm as the pyrolysis temperature is raised from 800° to 1200°C, with most of the decrease occurring between 800° and 1000°. This decrease may be interpreted as being due primarily to an increase in carrier mobility with pyrolysis temperature.
2. The resistivities of the pellets may be roughly doubled by appropriate Ca or Th doping, and halved by Na doping at a pyrolysis temperature of 800°, but they vary with doping level in a complex manner. Part of this variation may be ascribed to variations in pellet density, but most of it is probably due to the manner in which the impurity is distributed in the pyro-polymer. In any case, these variations are small compared to those which may be achieved through control of the pyrolysis temperature.
3. The materials all exhibit the negative resistivity-temperature dependence common to semi-conductors. Energy gaps are small, on the order of 0.005 to 0.05 ev, and decrease with pyrolysis temperature, reflecting an increase in carrier concentration as the pyrolysis temperature is raised.
4. These pyro-polymers are n-type semi-conductors, as indicated by Hall coefficient and qualitative thermoelectric power measurements.
5. The Hall coefficients are negative and very small (0 to -0.05 cm³/coul.). They appear to decrease slightly (become negatively larger) with both pyrolysis temperature and doping level.

6. The carrier densities for a typical 1000°C pyro-polymer are estimated to be on the order of $1-3 \times 10^{20}$ carriers/cm³, with mobilities of 2-4 cm²/v-sec. It may then be concluded that there is roughly one carrier per 140-500 carbon atoms in these materials.
7. X-ray data show the presence of crystalline structure, probably oxides or carbides, in the sodium and highly doped calcium pyro-polymers, while the lightly doped calcium and the thorium-doped materials exhibit the basically amorphous or micro-crystalline structure of the undoped pyro-polymers.

COMPARISON OF Ni¹, Al², Na, Ca,
and Th DOPED PYRO-POLYMERS

1. The resistivities decrease with pyrolysis temperature in a similar manner for all materials and are of similar magnitude (0.01 - 0.1 ohm-cm).
2. Aluminum doping raises the resistivity while nickel doping lowers it. At a pyrolysis temperature of 800°C, sodium lowers the resistivity, but at 1000° and 1200°, it causes a slight increase. Calcium is observed to first lower the resistivity slightly and then cause it to increase as the doping level is raised. Thorium, at a much lower maximum doping level than the others, produces an initial rise, but levels off with little change as the doping level is raised.
3. Sodium, calcium, thorium and aluminum-doped pyro-polymers exhibited negative resistivity-temperature behavior, while some of the nickel-doped samples had positive resistivity-temperature coefficients.
4. The energy gaps for all the pyro-polymers studied decreased with pyrolysis temperature, and were of the same order of magni-

tude (0 to 0.05 ev), with some nickel-doped samples showing metallic conduction (negative E_G).

5. Hall coefficients for Na, Ca, Al and Th-doped polymers were of the same order of magnitude (0 to 0.05 cm³/coul.) but those for Ni-doped materials were a factor of ten larger. Na, Ca and Th-doped materials had negative coefficients while the few measured for Al-doped polymers were positive. The majority of Hall coefficients of the Ni-doped polymers were positive, but those few which were negative agreed fairly well in magnitude with the Na, Ca and Th-doped materials.

6. Estimation of carrier densities and mobilities based on thermoelectric power measurements of aluminum-doped materials and Hall measurements of Na, Ca, or Th-doped polymers agree quite well at $n = 1-3 \times 10^{20} \text{ cm}^{-3}$

$$\mu = 1-4 \text{ cm}^2/\text{v-sec.}$$

These results differ slightly from those calculated from Hall measurements of nickel-doped pyro-polymers, primarily due to the larger Hall coefficients observed in the latter materials.

REFERENCES

1. H.A. Pohl and J.J. Hoglen, "Semiconduction in Nickel-Doped Polymer Carbons", Princeton University Plastics Laboratory Technical Report 53D, April 1959.
2. H.A. Pohl and J.P. Laherrere, "Semiconduction in Aluminum-Doped Pyro-Polymers", Princeton University Plastics Laboratory Technical Report 57C, April 1960.
3. H.A. Pohl, "Semi-Conduction in Polymers", Princeton University Plastics Laboratory Technical Report 61D, March 1961.
4. S. Mrozowski, "Electric Resistivity of Interstitial Compounds of Graphite", J. Chem. Phys., 21, 3 (1953).
5. S. Mrozowski, "Semiconductivity and Diamagnetism of Polycrystalline Graphite and Condensed Ring Systems", Phys. Rev., 35, 609 (1952) and 36, 1056 (1952).
6. H. Pinnick, "Electrical Properties of Graphite and Carbons", p. 3, Proceedings of the First and Second Conferences on Carbon, Mrozowski and Phillips, eds., Baltimore, Waverly (1956).
7. E.E. Loebner, "Thermoelectric Power, Electrical Resistance, and Crystalline Structure of Carbons", Phys. Rev., 102, 46-57 (1956).
8. C.A. Klein, "Electrical Properties of Pyrolytic Graphites", Raytheon Company, Research Division Technical Report R-58, February 1961.
9. F. Winslow, W. Baker, N. Pope and W. Matreyek, "Formation and Properties of Polymer Carbons", J. Poly. Sci., 16, 101 (1955).
10. Hannay, "Semiconductors", p. 36, New York, Reinhold (1959).
11. N. Cusack, "The Electrical and Magnetic Properties of Solids", p. 210, London, Longmans, Green and Co., (1958).
12. Ibid., p. 216.
13. McDougall and Stoner, Phil. Trans. Roy. Soc., (London), A237, 350 (1938).
14. J.H. Perry, ed., "Chemical Engineers' Handbook", p. 289, New York, McGraw-Hill (1950).
15. "Handbook of Chemistry and Physics", 37th ed., p. 1959-61, Cleveland, Chemical Rubber Publishing Co. (1955).
16. Ibid., p. 591.
17. Ibid., p. 489.

18. F. Winslow, W. Baker and W. Yager, "Structures and Properties of Some Pyrolysed Polymers", p. 93, Proceedings of the First and Second Conferences on Carbon, Mrozowski and Phillips, eds., Baltimore, Waverly (1958).
19. E.R. Roberts and P.C.L. Thorne, "Fritz Ephriam Inorganic Chemistry", p. 864, New York, Interscience Pub. (1949).
20. T. Moeller, "Inorganic Chemistry", p. 697, New York, Wiley and Sons (1952).
21. T.C. Harman, "Measurement Techniques for Electrical Resistivity, Hall Coefficient, Seebeck Coefficient and Thermal Conductivity", MIT Lincoln Lab., 83G-0019, June 1960.
22. A.J. Rosenberg, "Activity Coefficients of Electrons and Holes at High Concentrations", J. Chem. Phys., 33, 3, 665-667 (1960).
23. G.H. Hennig, "The Properties of the Interstitial Compounds of Graphite. III. The Electrical Properties of the Halogen Compounds of Graphite", J. Chem. Phys., 20, 9, p. 1443-1447 (1952).
24. M.L. Dzurus and G.R. Hennig, "Properties of the Interstitial Compounds of Graphite IV. Properties of N-Type Compounds", J. Chem. Phys., 27, 1, p. 275-281 (1957).
25. Cusack, opcit., p. 213.
26. H.A. Pohl and J.P. Laherrere, "Carrier Behavior in Nickel-Doped Polymer Carbons", Princeton University Plastics Laboratory Technical Report 54A, June 1959.
27. Cusack, opcit. p. 418.

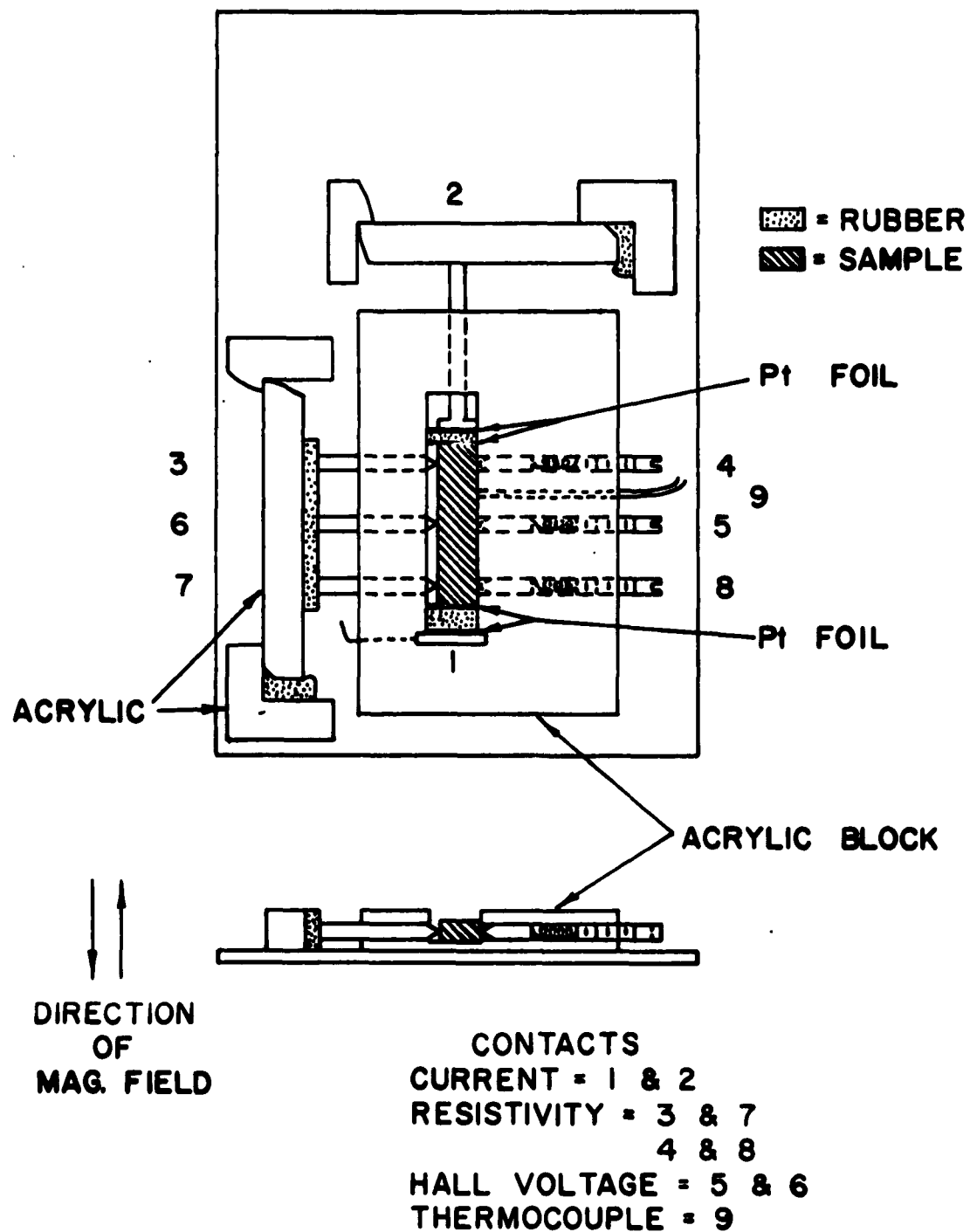
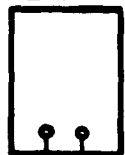


Fig. 1 Diagram of the cell used to measure resistivities and Hall voltages. Wires to contacts 2 - 8 are not shown.

**DECADE
RESISTANCE
BOX**

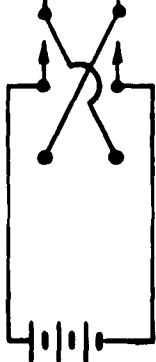


THERMOCOUPLE

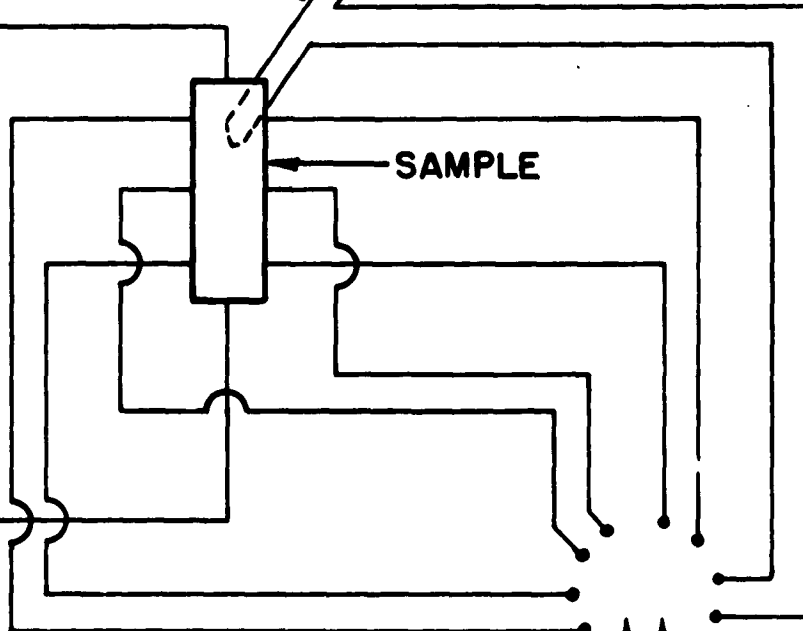


ICE BATH

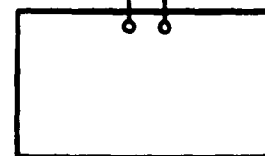
SAMPLE



DPDT



DP4T



POTENTIOMETER

Fig. 2 Electrical circuits.

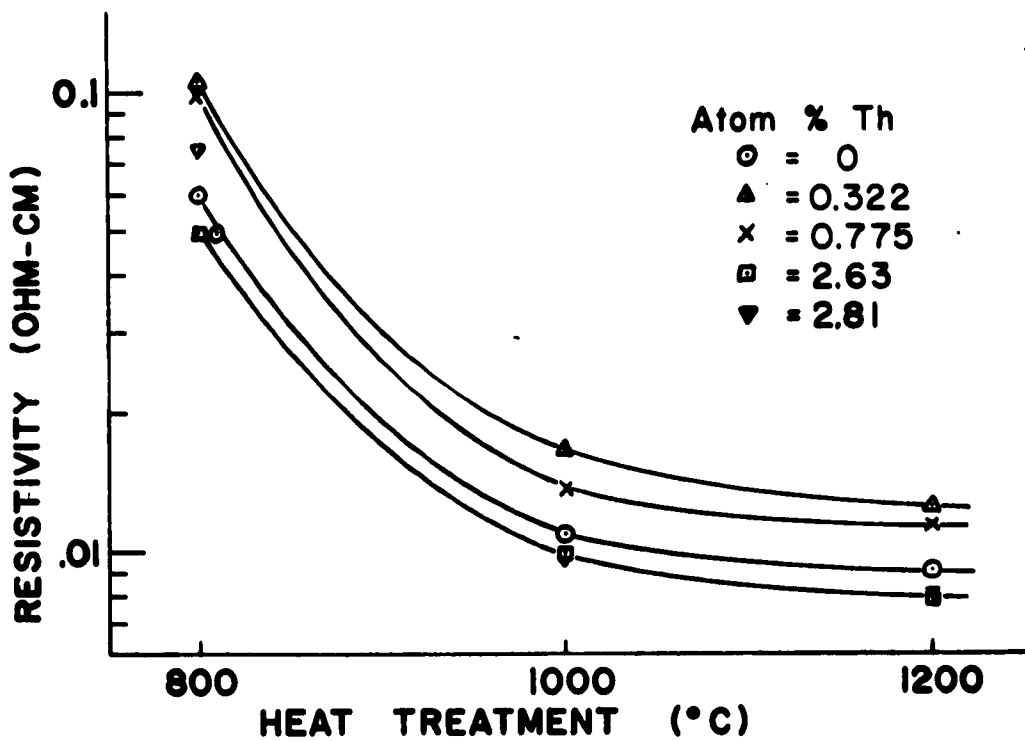
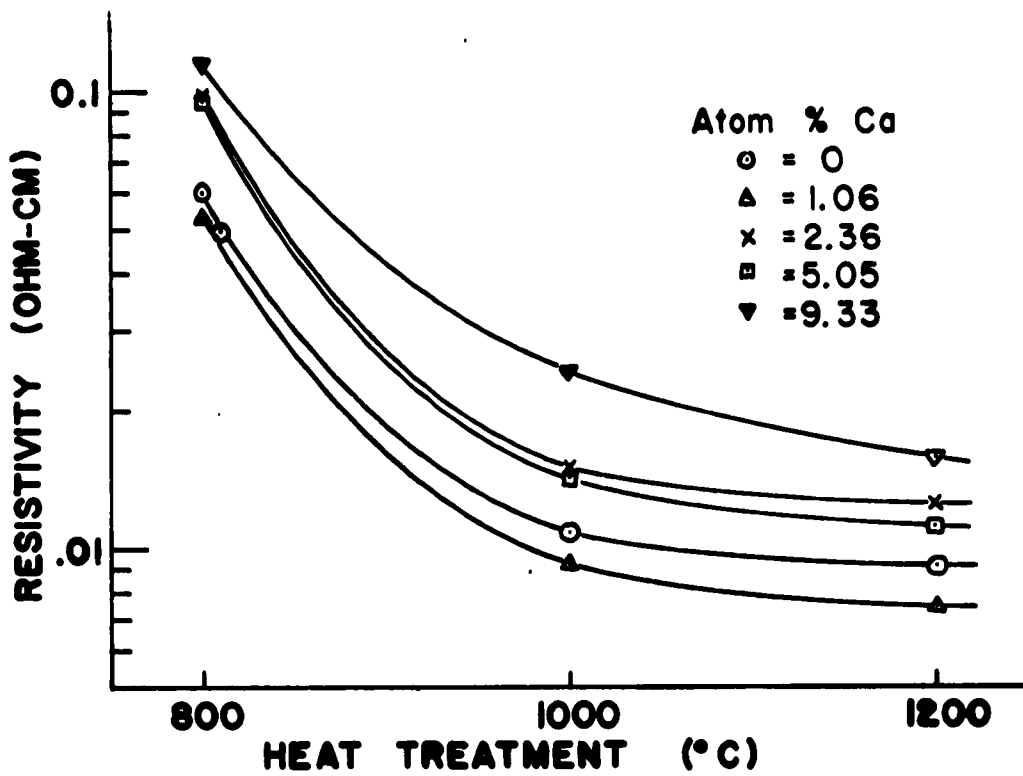


Fig. 3 Variation of pellet resistivity (uncorrected) with pyrolysis temperature.

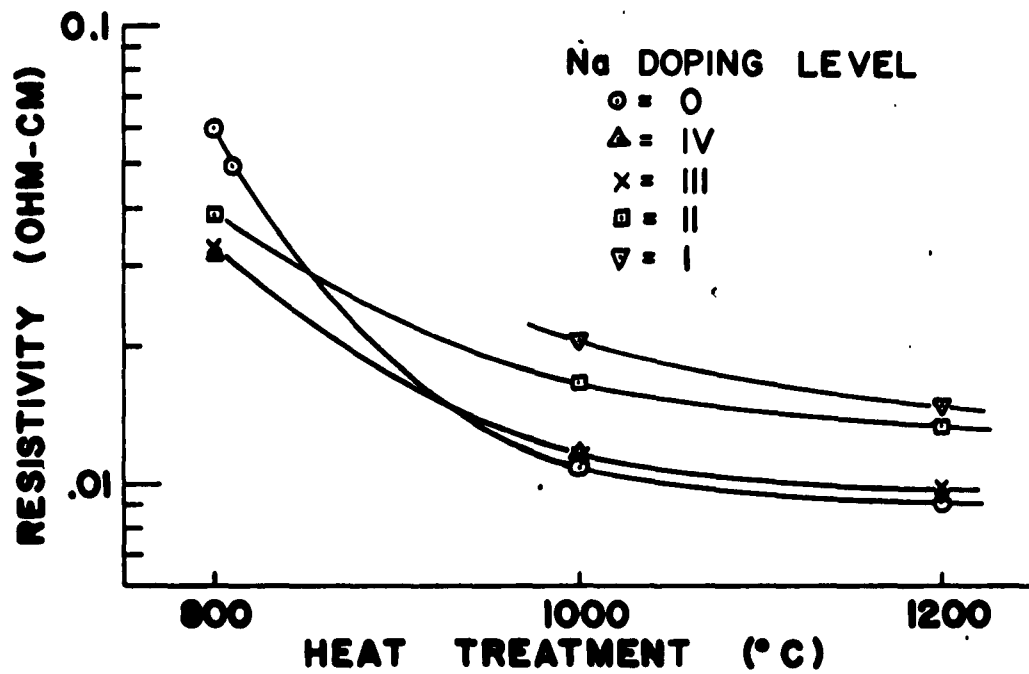


Fig. 3 Continued.

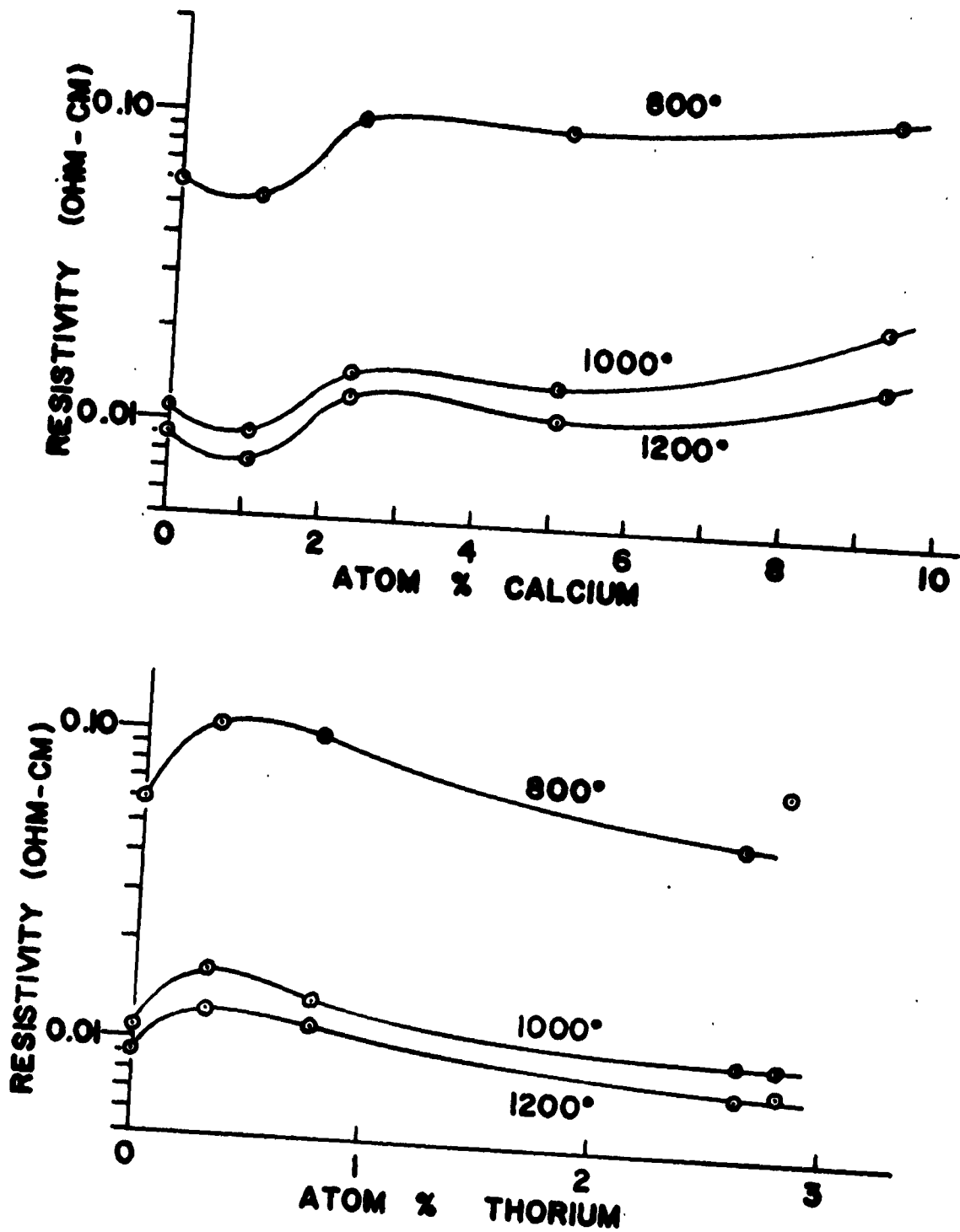


Fig. 4 Variation of pellet resistivity (uncorrected) with doping level.

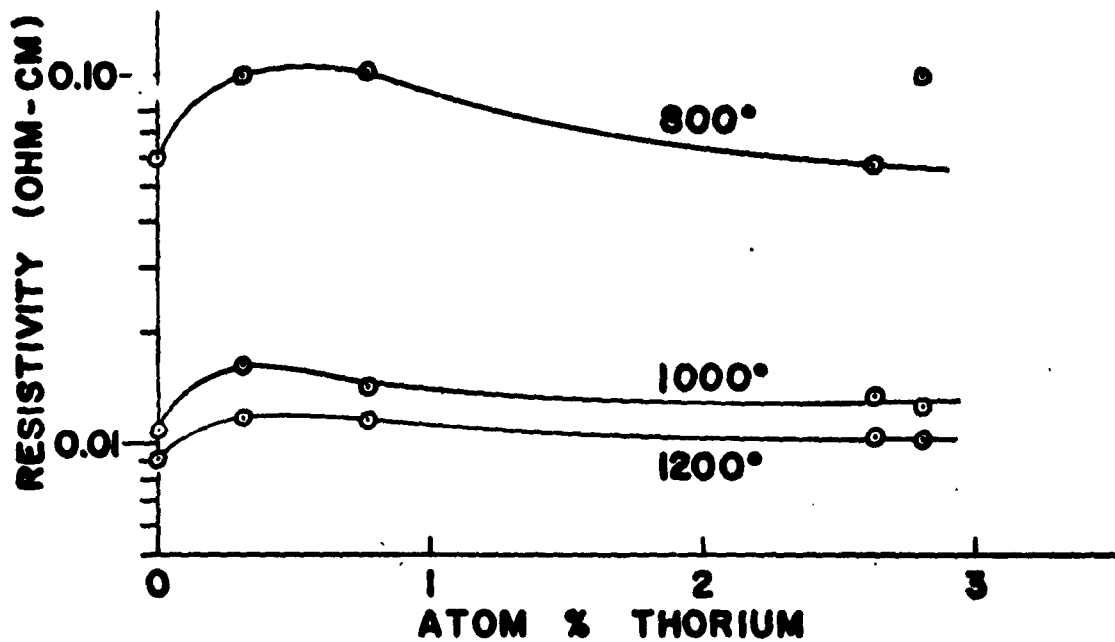
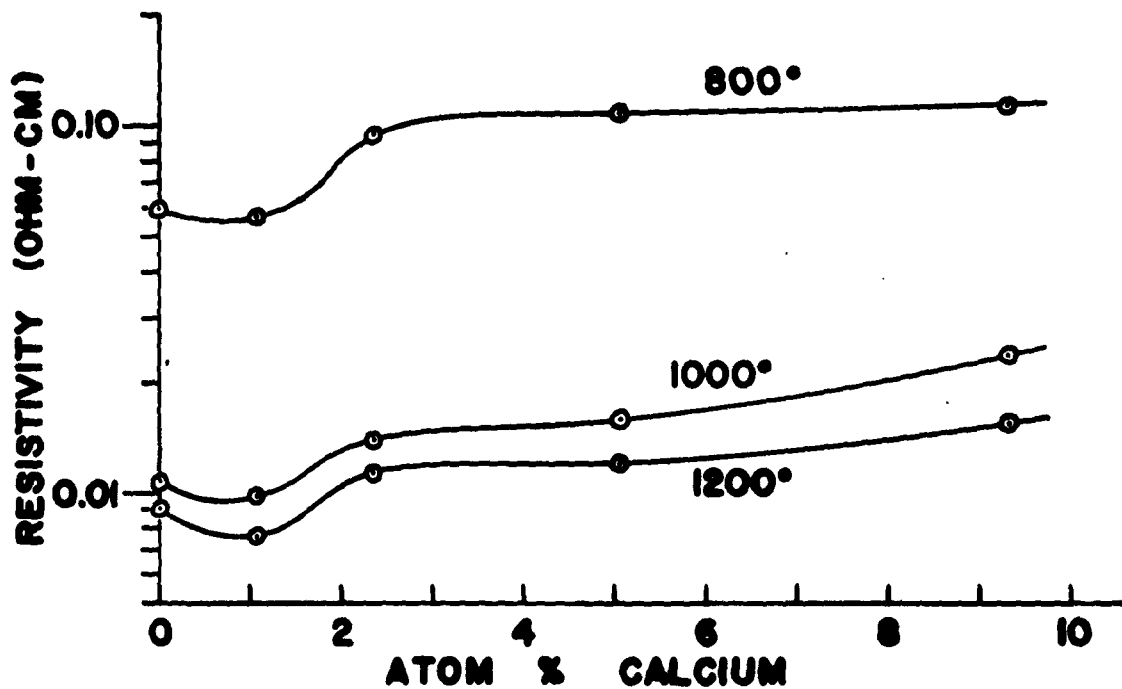
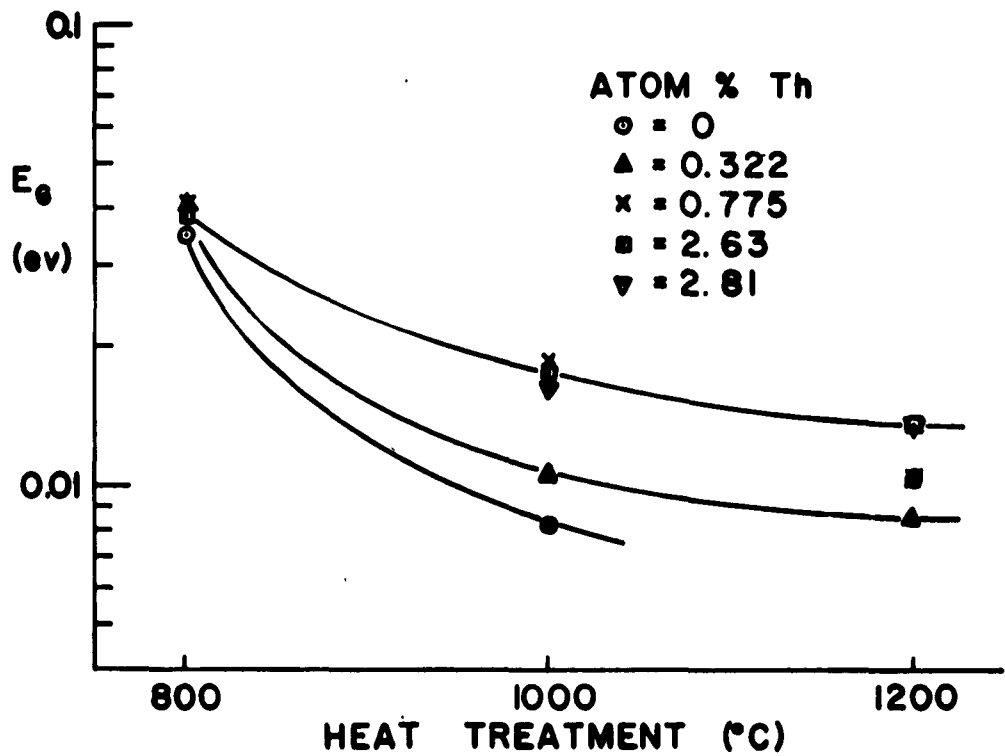
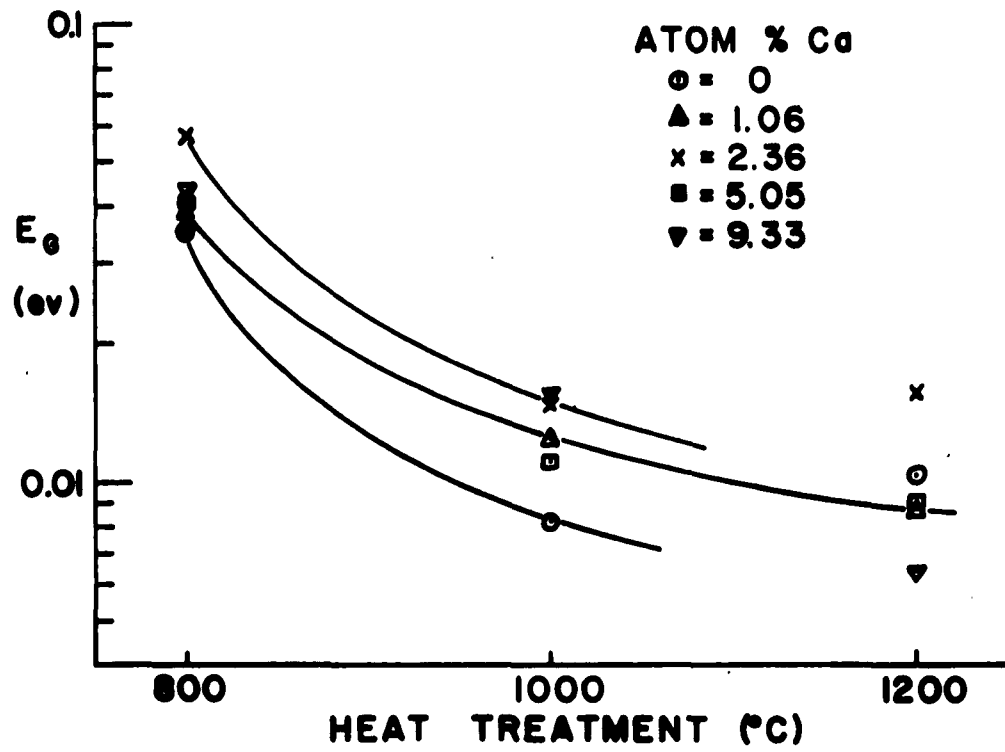


Fig. 5 Variation of resistivity with doping level. Resistivity values are corrected for variations in pellet density by procedure shown in Calculations section.

Fig. 6 Variation of energy gap with pyrolysis temperature.



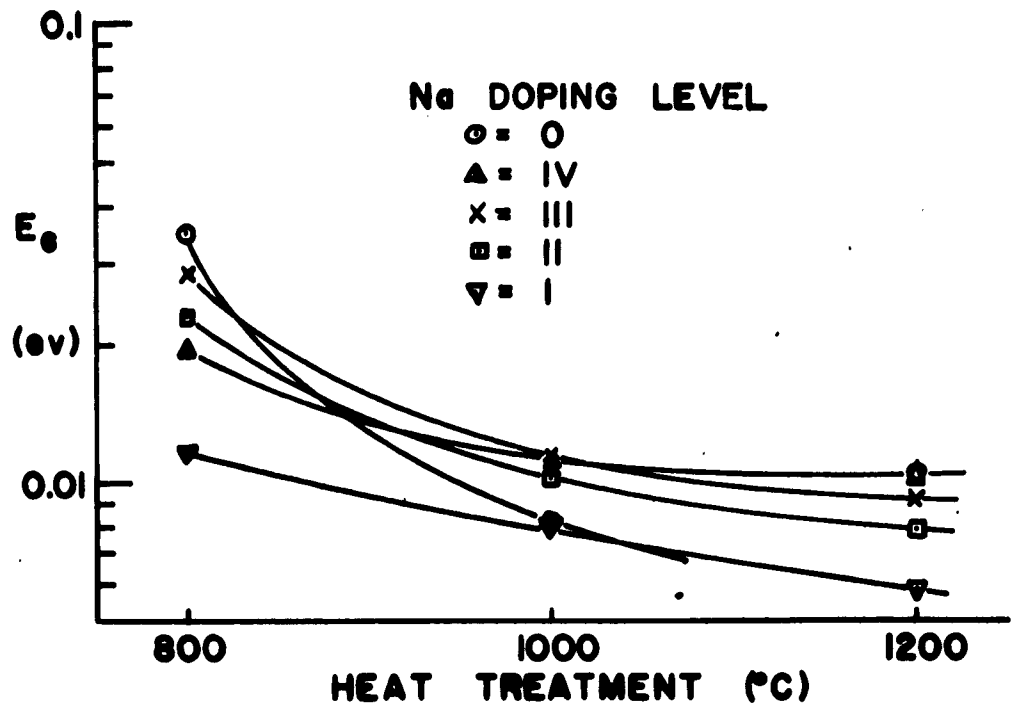


Fig. 6 Continued.

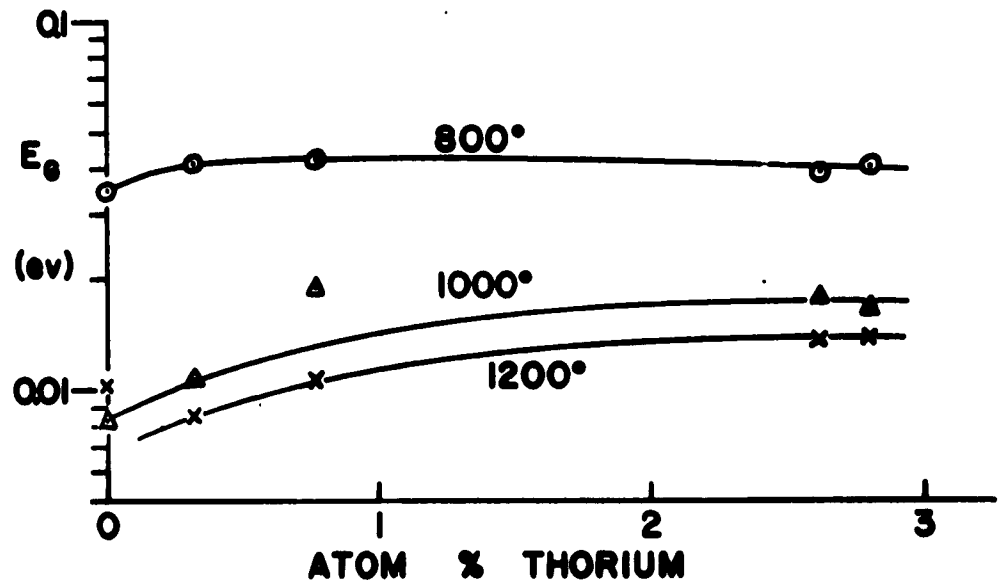
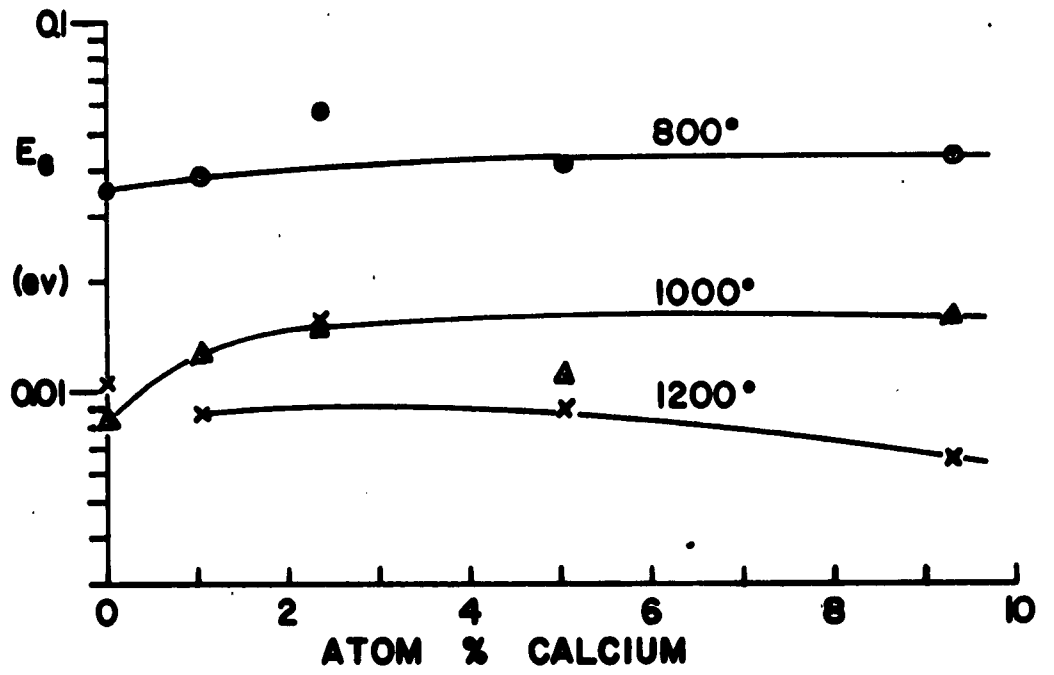


Fig. 7 Variation of energy gap with doping level.

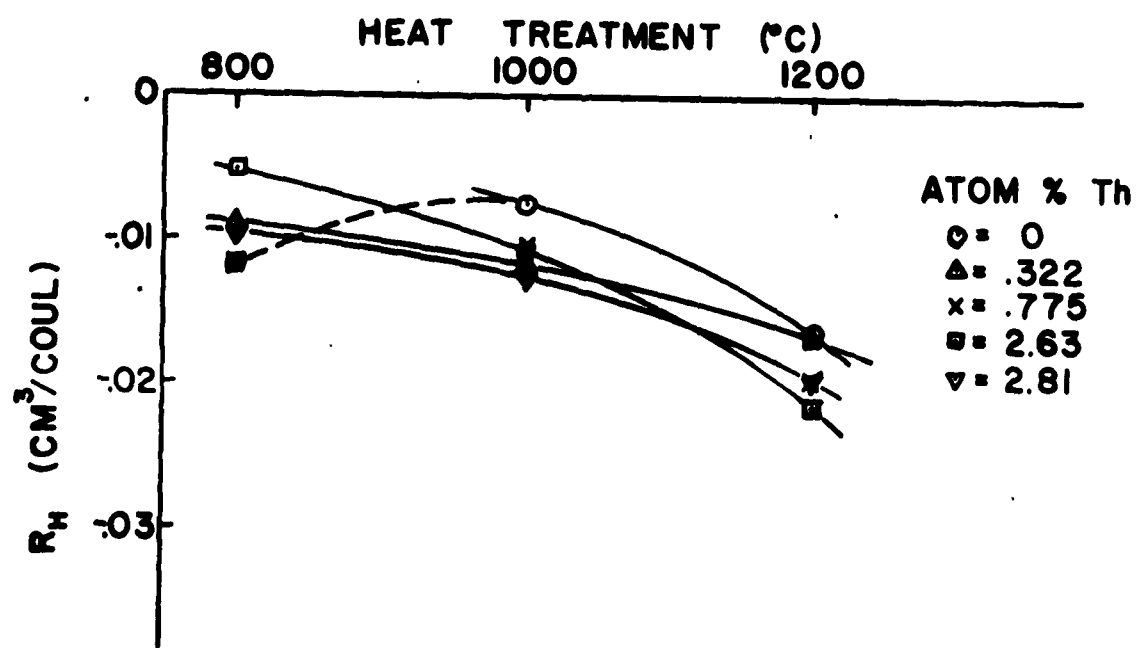
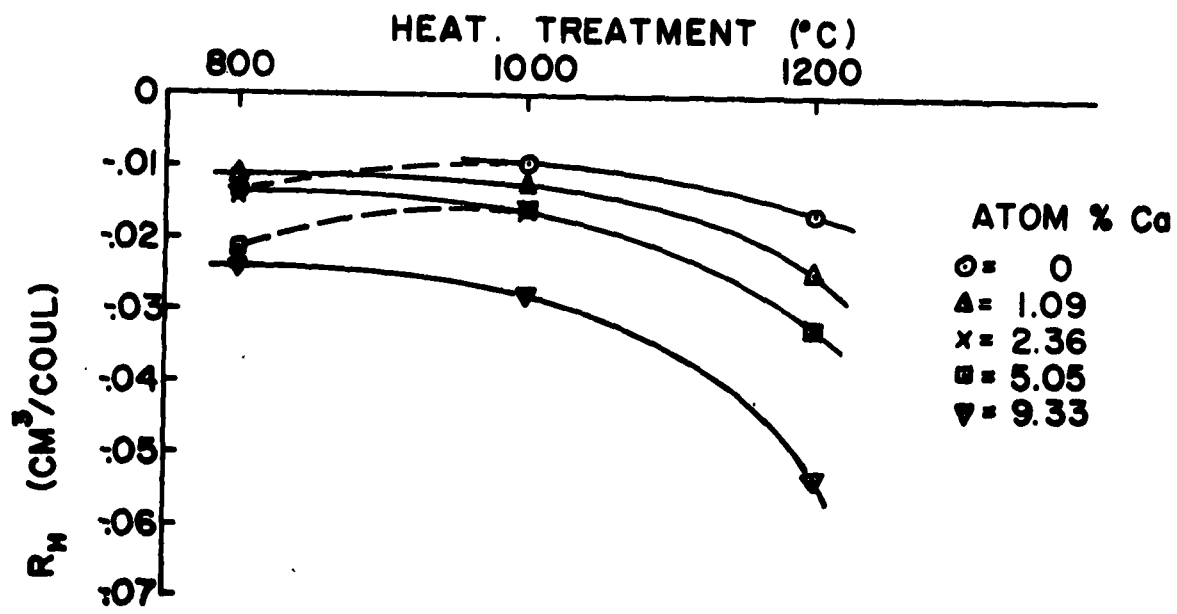


Fig. 8 Variation of Hall coefficient with pyrolysis temperature.

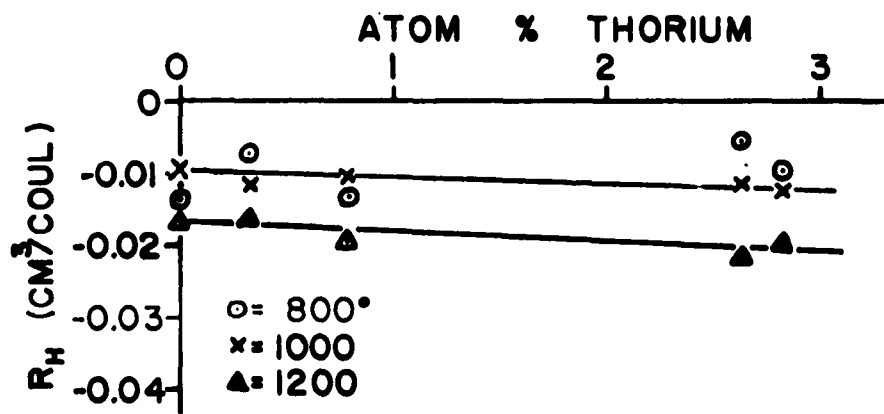
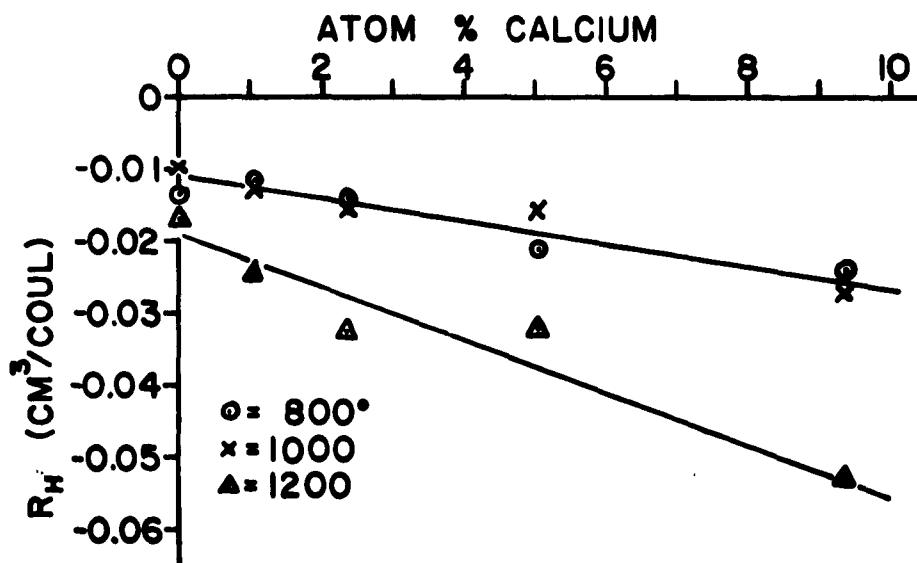


Fig. 9 Variation of Hall coefficient with doping level.

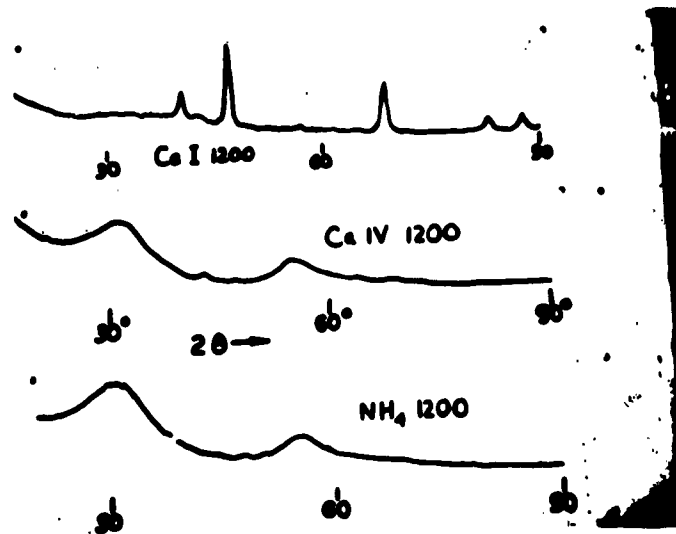


Fig. 10 X-ray spectrographs

PRINCETON UNIVERSITY

Distribution List for Technical Reports

Contract DA-36-039-SC-89143

1n. Commanding Officer
Office of Naval Res. Branch Office
The John Crerar Library Building
86 East Randolph Street
Chicago 1, Illinois (1)

2n. Commanding Officer
Office of Naval Res. Branch Office
346 Broadway
New York 13, New York (1)

3n. Commanding Officer
Office of Naval Res. Branch Office
1030 E. Green Street
Pasadena 1, California (1)

4n. Commanding Officer
Office of Naval Res. Branch Office
Navy No. 100
Fleet Post Office
New York, New York (7)

5n. Director, Naval Res. Lab.
Washington 25, D. C.
Attn: Technical Inform. Officer (6)
Chemistry Division (2)
Code 6110 (1)

6n. Chief of Naval Research
Department of the Navy
Washington 25, D. C.
Attn: Code 425 (2)

7n. Technical Library OASD(R&D)
Pentagon Room 3E1065
Washington 25, D. C. (1)

8n. Technical Director
Research & Engineering Div.
Office of the Quartermaster General
Department of the Army
Washington 25, D. C. (1)

9n. Research Director
Chemical & Plastics Division
Quartermaster Res. & Eng. Command
Natick, Massachusetts (1)

10n. Air Force
Office of Scientific Res.(SRLT)
Washington 25, D. C. (1)

11n. Commanding Officer
Diamond Ordnance Fuze Labs.
Washington 25, D. C.
Attn: Tech. Ref. Section
(ORDTL 06.33) (1)

12n. Office of Chief of Staff(R&D)
Department of the Army
Pentagon 3B516
Washington 25, D. C.
Attn: Chemical Adviser (1)

13n. Chief, Bureau of Ships
Department of the Navy
Washington 25, D. C.
Attn: Code 340 (2)

14n. Chief, Bur. of Naval Weapons
Department of the Navy
Washington 25, D. C.
Attn: Technical Library (3)
Code RRMA-3 (1)

15n. ASTIA
Document Service Center
Arlington Hall Station
Arlington 12, Virginia (10)

16n. Command. Officer
USASRDL
Fort Monmouth, New Jersey
Attn: SIGRA/SL-RE (1)

17n. Naval Radiological Defense
Laboratory
San Francisco 24, California
Attn: Technical Library (1)

18n. Naval Ordnance Test Station
China Lake, California
Attn: Head, Chem. Div. (1)
Code 40 (1)
Code 50 (1)

19n. Commanding Officer
U.S. Army Research Office
Box CM, Duke Station
Durham, North Carolina (1)
Attn: CRD-AA-IP-Mr. Ulah

20n. Brookhaven National Lab.
Chemistry Division
Upton, New York (1)

21n. Atomic Energy Commission
Research Division
Chemistry Branch
Washington 25, D. C. (1)

22n. Atomic Energy Commission
Library Branch
Technical Information ORE
Post Office Box E
Oak Ridge, Tennessee (1)

23n. U.S. Army Chem. Warfare Labs.
Technical Library
Army Chemical Center, Maryland (1)

24n. Office of Technical Services
Department of Commerce
Washington 25, D. C. (1)

25n. Commanding Officer
Naval Air Development Center
Johnsville, Pennsylvania
Attn: Dr. Howard R. Moore (1)

26n. Mr. M. Lipnick
Diamond Ordnance Fuze Laboratory
Washington 25, D. C. (1)

27n. Naval Powder Factory
Indian Head, Maryland
Attn: Mr. A. F. Johnson (1)

28n. Naval Electronics Laboratory
San Diego, California (1)

29n. Naval Ordnance Laboratory
Silver Springs, Maryland
Attn: Dr. Albert Lightbody (1)

30n. Materials Laboratory
New York Naval Shipyard
Brooklyn, New York (1)

31n. Commander
Mare Island Naval Shipyard
Rubber Laboratory
Vallejo, California (1)

32n. Naval Air Experiment Station
Philadelphia Naval Shipyard
Philadelphia 12, Pa. (2)

33n. Dr. J. H. Faull, Jr.
72 Fresh Pond Lane
Cambridge, Mass. (1)

34s. Dr. Gregg Andrus
OC Sig. O, R&D Division
Washington 25, D. C.
Attn: SIGKD 4A (1)

35n. Dr. A. V. Tobolsky
Department of Chemistry
Princeton University
Princeton, New Jersey (1)

36n. Dr. W. Heller
Wayne State University
Detroit, Michigan (1)

37n. Dr. U. P. Strauss
Department of Chemistry
Rutgers University
New Brunswick, New Jersey (1)

38n. Dr. E. G. Rochow
Department of Chemistry
Harvard University
Cambridge 38, Mass. (1)

39n. Dr. E. G. Wallace
Stauffer Chemical Company
1375 S. 47th Street
Richmond, California (1)

40n. Dr. R. S. Stein
Department of Chemistry
University of Massachusetts
Amherst, Mass. (1)

41n. Dr. H. C. Brown
Department of Chemical Engineering
Engineering & Ind. Exper. Station
University of Florida
Gainesville, Florida (1)

42n. Mr. J. B. Rust
Hughes Aircraft Company
Culver City, California (1)

43n. Dr. Leo Mandelkern
National Bureau of Standards
Washington 25, D. C. (1)

44n. Stauffer Chemical Company
Molded Products Division
3211 E. 26th Street
Los Angeles 23, California
Attn: Dr. John McColgan (1)

45n. Dr. G. Barth-Wehrenalp
Pennsalt Chemicals Corporation
P. O. Box 4388
Philadelphia 18, Pa. (2)

46n. Commanding Officer & Director
U.S. Naval Civil Engineering Lab.
Port Hueneme, California
Attn: Chemistry Division (1)

47n. Dr. T. G. Fox
Mellon Institute
4400 Fifth Avenue
Pittsburgh 13, Penna. (1)

48n. Dr. Riley Schaeffer
Department of Chemistry
Indiana University
Bloomington, Indiana (1)

49n. Library
Textile Research Institute
P. O. Box 625
Princeton, New Jersey (1)

50n. Plastics Tech. Eval. Center
Picatinny Arsenal
Dover, New Jersey (1)

51s. Commanding Officer
Engineer R&D Labs.
Fort Belvoir, Virginia
Attn: Document Center (1)

52s. Commanding Officer
U.S. Army Signal R&D Lab.
Fort Monmouth, New Jersey
Attn: SIGRA/SL-ADT (1)

53s. Commanding Officer
U.S. Army Signal R&D Lab.
Fort Monmouth, New Jersey
Attn: SIGRA/SL-ADJ (File Unit No. 3,
ECR Dept.) (1)

54s. Commanding Officer
U.S. Army Signal R&D Lab.
Fort Monmouth, New Jersey
Attn: SIGRA/SL-TN (FOR RETRANS-
MITTAL TO ACCREDITED BRITISH & (3)
CANADIAN GOVERNMENT REPRESENTATIVES)

55s. Commanding Officer
U.S. Army Signal Equip. Support Agcy.
Fort Monmouth, New Jersey
Attn: SIGMS/ADJ (1)

56s. Commanding Officer
U.S. Army Signal Equip Support Agcy.
Fort Monmouth, New Jersey
Attn: SIGMS-SDM (1)

57s. Commanding Officer
U.S. Army Signal R&D Lab.
Fort Monmouth, New Jersey
Attn: SIGFM/EL-P (1)

58s. Commander
Air Force Command & Control Div.
Air R&D Command
U.S. Air Force
L.G. Hanscomb Field
Bedford, Mass.
Attn: CROTIR-2 (1)

59s. Commander
Rome Air Development Center
Air R&D Command
Griffiss AFB, New York
Attn: RCSSID (1)

60s. Commanding Officer
U.S. Army Signal R&D Labs.
Fort Monmouth, New Jersey
Attn: SIGRA/SL-PE (1)

61s. Commanding Officer
U.S. Army Signal R&D Labs.
Fort Monmouth, New Jersey
Attn: SIGRA/SL-PEM (1)

62s. Advisory Group on Electronic
Parts

Moore School Building
200 South 33rd Street
Philadelphia 4, Pa. (4)

63s. Commanding General
Army Ordnance Missile Command
Signal Office
Redstone Arsenal, Alabama (1)

64s. General Electric Company
Research Laboratory
P. O. Box 1088
Schenectady, New York
Attn: Dr. A. M. Bueche (1)

65s. Tech. Information Center
Lockheed Missiles & Space Div.
3251 Hanover Street
Palo Alto, California
Attn: Mr. W. A. Kozumplik (1)

66s. U.S. Army Signal Liaison Office
Aeronautical Systems Division
ATTN: ASDL-9

Wright-Patterson AFB, Ohio (2)

67s. USNSRD, Facilities
Clothing & Textile Division
3rd Avenue & 29th Street
Brooklyn 32, N.Y. (Librarian) (1)

68s. C. O. USASRDL
Fort Monmouth, New Jersey
Attn: SIGRA/SL-XE
Dr. H. H. Kedesdy (1)

69s. C. O. USASRDL
Fort Monmouth, New Jersey
Attn: SIGRA/SL-PDP
Dr. H. Mette (1)

70s. Chief, U.S. Security Agcy.
Arlington Hall Station
Arlington 12, Virginia (2)

71s. Deputy President, U.S.A.
Security Agency Board
Arlington Hall Station
Arlington 12, Virginia (1)

72s. Space Technology Labs.
P. O. Box 95001
Los Angeles 45, California (1)

73s. Dr. M. S. Cohen, Chief
Propellants Synthesis Section
Reaction Motors Division
Denville, New Jersey (1)

74s. Boeing Airplane Company
Transport Division
P. O. Box 707
Renton, Washington
Attn: Mr. F.N. Markey, Unit Chief (1)

75s. Commanding Officer
Ordnance Materials Res. Office
Watertown Arsenal
Watertown 72, Mass.
Attn: RPD (1)

76s. Commanding Officer
Rock Island Arsenal
Rock Island, Illinois
Attn: Mr. R. Shaw, Laboratory (1)

77s. Monsanto Chemical Company
Research & Engineering Div.
Boston 49, Massachusetts
Attn: Mr. K. Warren Easley (1)

78s. R. R. Sowell, Dept. 1110
Sandia Corp.
Albuquerque, New Mexico (1)

79s. L. M. Berry, Organ. 8115
Sandia Corp.
Livermore, California (1)